



Lymphoma

Characteristic gene alterations in primary gastrointestinal T- and NK-cell lymphomas

Gunho Lee^{1,2} · Hyang Joo Ryu³ · Ji Woon Choi⁴ · Hyundeok Kang^{1,5} · Woo Ick Yang³ · In Seok Yang¹ · Mi-kyoung Seo^{1,5} · Sangwoo Kim^{1,5} · Sun Och Yoon³

Received: 12 July 2018 / Revised: 22 September 2018 / Accepted: 22 October 2018 / Published online: 23 January 2019
© The Author(s) 2019. This article is published with open access

To the Editor:

Systemic T and natural killer (NK) cell lymphomas (systemic TNKs) are malignancies stemming from lymphocytes of T- and NK-cell lineage that preferentially occur in East Asians. Despite an aggressive nature and poor patient outcomes, their rarity and histological heterogeneity have limited the development of effective therapeutic options. Several subtypes have been described for TNKs according to their cellular origin and site of occurrence: these include angioimmunoblastic T-cell lymphoma (lymph nodes) and extranodal NK/T-cell lymphoma (ENKTL) (nasal/paranasal sites of the head/neck). Some TNKs, such as enteropathy-associated T-cell lymphoma or monomorphic

epitheliotropic intestinal T-cell lymphoma (MEITL), are frequently found along the gastrointestinal (GI) tract and are known to be more aggressive, with patients experiencing bleak clinical outcomes [1]. While this might indicate a site-specific preference in the formation and progression of TNKs, the molecular biology underlying such preference has not been fully elucidated. In this study, we sought to investigate genetic alterations in primary GI-TNKs in a comparative manner to characterize the molecular features thereof and to gain insights into the site-specific tumorigenesis of TNKs.

From Severance Hospital Cancer Registry data, 18 primary GI-TNKs were collected: GI-TNKL was defined according to the definitions proposed by Lewin et al. and the fourth revision of World Health Organization classification [1, 2]. The 18 cases consisted of six MEITLs, six ENKTLs, three anaplastic large cell lymphomas, and three intestinal T-cell lymphomas not otherwise specified (ITCL-NOS). In addition, 28 cases of non-GI-TNKL were collected for comparative analysis. The complete list of samples, clinical/pathological features, and overall workflow for sample collection are described in the accompanying Supplementary Data (Supplementary Tables 1 and 2, Supplementary Figures 1–3, and Supplementary Appendix).

Initially, we conducted whole-exome sequencing (WES) analysis for six GI-TNKL samples (three MEITLs and three ENKTLs) to obtain a rough profile of somatic mutations. After assessment of the data quality (Supplementary Table 3), we applied the Genome Analysis Toolkit best practice pipeline on the WES data to discover somatic variants (Supplementary Figure 4 and Supplementary Appendix) and identified 230 genes with somatic mutations. We also conducted a literature survey to obtain additional gene variants: mutations in 187 lymphoma-related genes were reported in previous genomic studies (Supplementary Figure 5A). Finally, we constructed a targeted panel of 417 genes for deeper analysis of GI- and non-GI-TNKs (Supplementary Table 4).

These authors contributed equally: Gunho Lee, Hyang Joo Ryu

These authors jointly supervised this work: Sangwoo Kim, Sun Och Yoon

Supplementary information The online version of this article (<https://doi.org/10.1038/s41375-018-0309-4>) contains supplementary material, which is available to authorized users.

✉ Sangwoo Kim
swkim@yuhs.ac

✉ Sun Och Yoon
soyoon@yuhs.ac

¹ Department of Biomedical Systems Informatics, Yonsei University College of Medicine, Seoul, Republic of Korea

² Graduate Program for Nanomedical Science, Yonsei University, Seoul, Republic of Korea

³ Department of Pathology, Yonsei University College of Medicine, Severance Hospital, Seoul, Republic of Korea

⁴ Department of Pathology, Yonsei University Wonju College of Medicine, Wonju, Republic of Korea

⁵ Brain Korea 21 PLUS Project for Medical Science, Yonsei University College of Medicine, Seoul, Republic of Korea

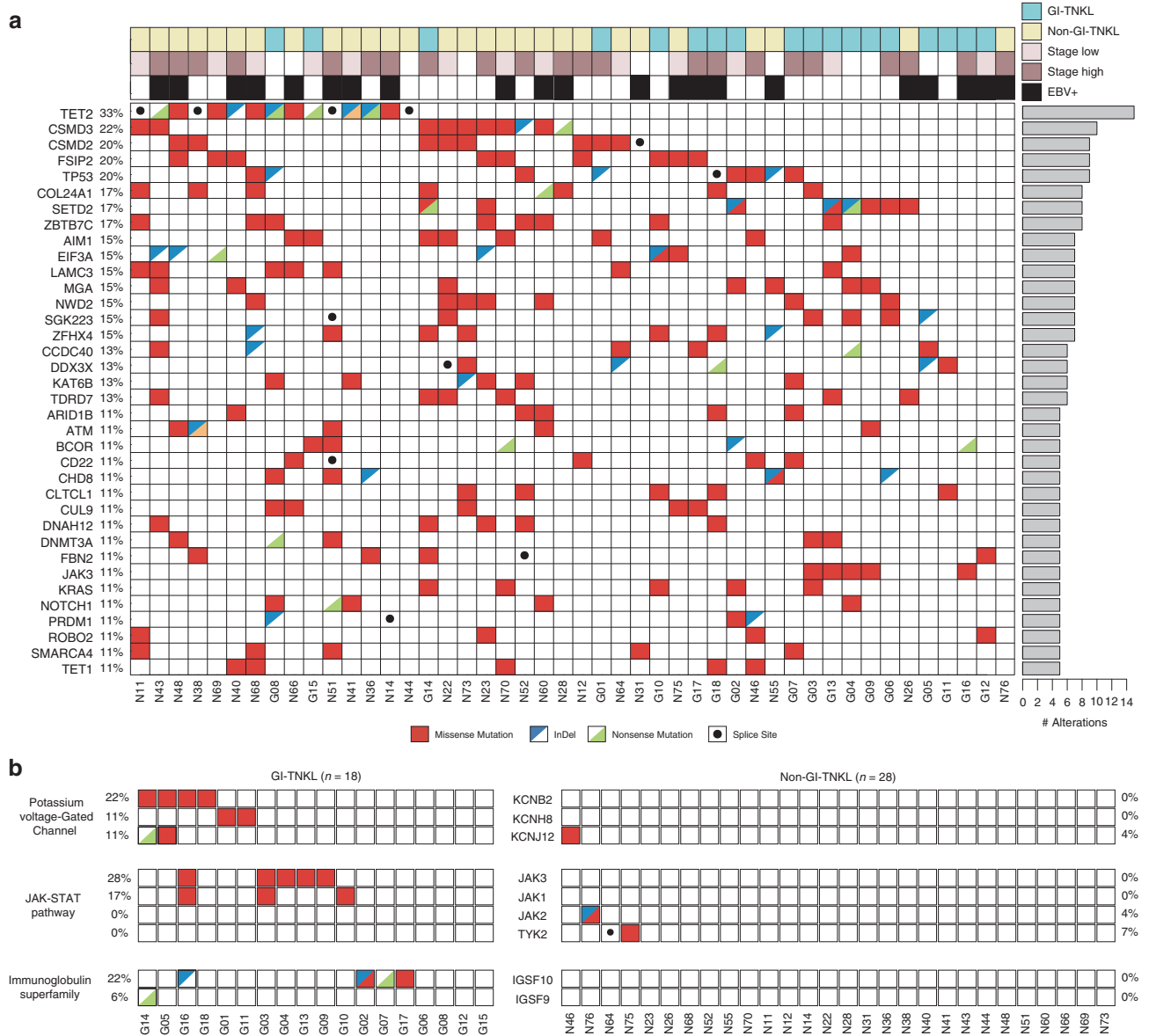


Fig. 1 Genomic landscape of alterations in GI-TNKL and non-GI-TNKL. **a** Distribution of well-known somatic alterations in 46 GI-TNKL and non-GI-TNKL patients. Sites of origin (GI-TNKL = sky blue, non-GI-TNKL = yellow), stages (high = brown, low = pink), and EBV positivity (black) are displayed along the top. Individual patients and cancer type (GI-TNKL [G] or non-GI-TNKL [N]) are indicated at the bottom. Frequencies of the mutations in the study

population are displayed on the left side of the table. Bars on the right show the total numbers of alterations in each gene. Mutation types are indicated in different colors: missense (red), indel (blue triangle), nonsense (green triangle), or splice site (black dot). **b** Alteration landscape showing recurrent distributions of mutations in key pathways discovered in GI-TNKL patients

Using the targeted panel, we conducted deep targeted sequencing ($\sim 900\times$) for 46 TNKL samples (18 GI- and 28 non-GI-TNKLs) (Supplementary Figure 5B and Supplementary Appendix). At this stage, we applied more stringent filtering for genes from large public germline databases and frequent false positive genes (referred to as “blacklist” genes) (Supplementary Figure 4, Supplementary Table 5, and Supplementary Appendix). This variant analysis identified 880 nonsynonymous somatic mutations at 833 unique

sites (19.1 total and 18.1 unique mutations per patient) (Supplementary Tables 6 and 7). We assumed that a high mutation load (8.02/Mb) resulted from the targeted sequencing. Mutation spectrums, base-substitution frequency ($C > T$ enriched), and Ti/Tv ratio (~ 2.6) were similar between GI- and non-GI-TNKLs and reflected the typical characteristics of cancers (Supplementary Figures 6 and 7).

Inspecting the genetic landscape of nonsynonymous mutations (Fig. 1a), we discovered that *TET2* was the most

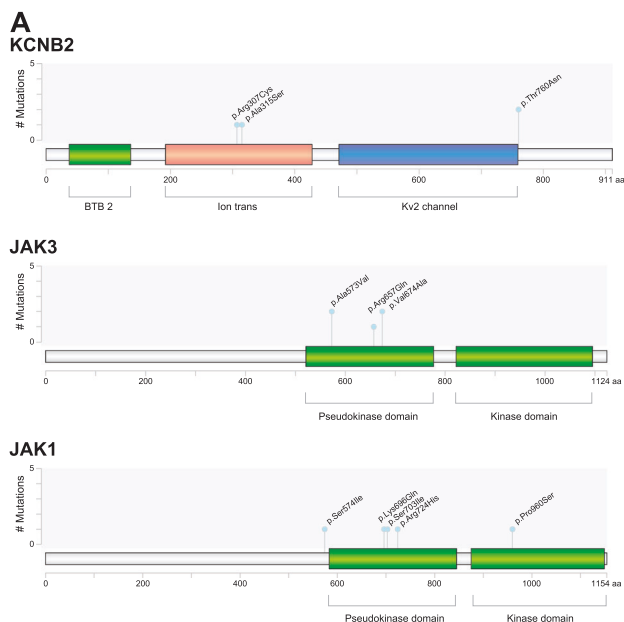
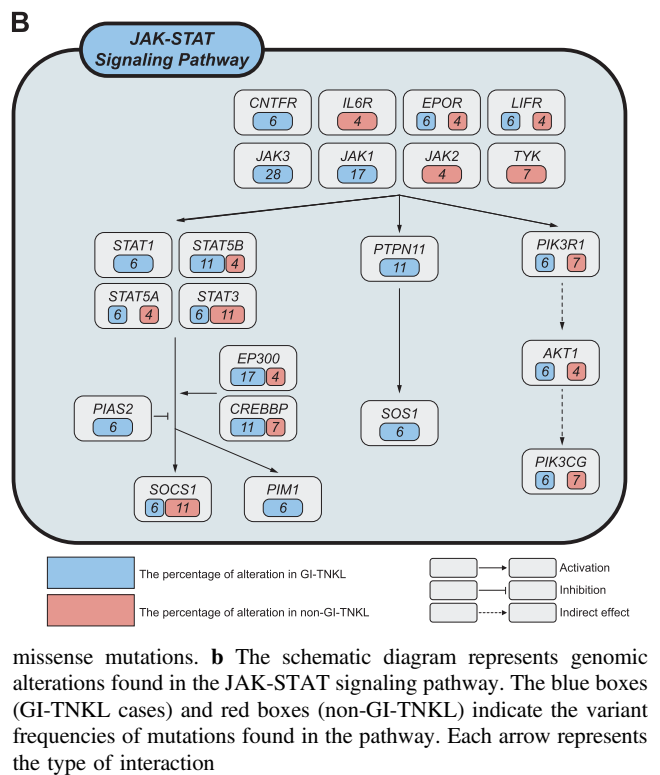


Fig. 2 *KCNB2*, *JAK3*, and *JAK1* lollipop plot and the JAK-STAT signaling pathway. **a** *KCNB2*, *JAK3*, and *JAK1* lollipop plots. The diagrams represent the protein domains of *KCNB2*, *JAK3*, and *JAK1* genes. Mutations are plotted along the x-axis, and the numbers of the mutations presented along the y-axis. Blue dots indicate individual

frequently mutated gene in all TNKL samples (15/46, 33%), followed by *CSMD3* (10/46, 22%), *CSMD2* (10/46, 20%), *FSIP2* (10/46, 20%), and *TP53* (9/46, 20%). Frequent indels, nonsense mutations, and splice site variants in *TET2* (10/15, 66%) and *TP53* (4/9, 44%) implied that mutations in these tumor suppressor genes may act in a loss-of-function manner. *SETD2* mutations were also observed in 17% of samples, corresponding to previous reports [3].

We further analyzed the site-specificity of the detected mutations (Fig. 1b). While previously known mutant genes were highly present in non-GI-TNKLs (46, 32, and 25% for *TET2*, *CSMD3*, and *CSMD2*, respectively), we were able to find a few novel mutations enriched in GI-TNKLs that are important in three different biological functions: the voltage-gated potassium (Kv^+) channel, the JAK-STAT pathway, and the immunoglobulin superfamily (see below).

With regard to Kv^+ channel pathway genes, eight mutations (seven missense and one nonsense single nucleotide variants) in *KCNB2* (4/18, 22%), *KCNH8* (2/18, 11%), and *KCNJ12* (2/18, 11%) were discovered in six GI-TNKL samples. These genes encode Kv^+ channel proteins that mediate transmembrane potassium transport in excitable membranes, which is primarily activated in brain and smooth muscle cells of the GI-tract [4]. Further analysis demonstrated that the *KCNB2* mutations were located in the ion transport and Kv2 channel domains (Fig. 2a). In silico protein modeling and multiple sequence alignment predicted that one of the *KCNB2* mutations (Arg307Cys)



results in a critical defect in the function of voltage-gated channels (Supplementary Figures 8, 9 and Supplementary Appendix), while the others remained inconclusive. Compared to normal tonsil tissue, non-GI-TNKL tissue, and GI-TNKL tissue with wild-type *KCNB2*, GI-TNKL tissue with *KCNB2* mutation exhibited lower levels of *KCNB2* mRNA upon reverse transcription PCR, although statistical significance was not observed (Supplementary Figure 10 and Supplementary Appendix). Immunohistochemical protein expression was correlated with mRNA expression of *KCNB2*. Also, low expression of *KCNB2* protein was found to be related with an inferior overall survival rate in systemic mature T- and NK-cell lymphomas regardless of GI or non-GI site (Supplementary Table 8, Supplementary Figure 11 and Supplementary Appendix).

Associations between altered regulation of the Kv^+ channel and cancer development have been continuously reported, such as mutations of *KCNH1* in breast cancer and acute myeloid leukemia [5, 6], of *KCNH2* in glioblastoma [7], and of *KCNA3* in pancreatic cancer [8]. In T cells, aberrations of Kv^+ channels have been shown to induce changes in intracellular K^+ and Ca^+ concentrations and to impair T-cell receptor-driven Akt-mTOR signaling and Ca^{2+} signaling pathways, thereby triggering T-cell activation [9]. In addition, such aberrations may induce a blockade of T-cell effector function by eliciting an ionic checkpoint, which results in immune suppression within the tumor microenvironment [9]. Thus, we conjectured that the

newly found mutations in the Kv⁺ channel family genes might be a potential driving mechanism of T-cell lymphoma and cancer immunity. Moreover, we suspect that the site-specificity of the mutations may mirror differences in the tumor microenvironment, considering the known functional roles of Kv⁺ channels in the GI tract, including electrolyte and substrate transport, cell migration, cell proliferation, and apoptosis [10].

The JAK-STAT pathway is a well-known mutation target in systematic TNKs [11–14]. In the present study, mutations in the JAK-STAT pathway showed GI specificity by presenting only in *JAK3* (5/18, 28%) and *JAK1* (3/18, 17%). Most previous studies have reported *JAK2* mutations only. The newly found *JAK3* and *JAK1* mutations were located in the pseudokinase and kinase domains (Fig. 2a). Further, we found more GI-specific mutations in the downstream genes of JAK-STAT pathways, including *STAT1*, *PTPN11*, and *SOS1*, which might indicate GI-TNKL-specific aberrations in the pathway (Fig. 2b). Although further study should follow, these findings suggest that differences in the tumor microenvironment might be related with the vulnerability of GI-TNKLs to genetic mutations in *JAK3* and *JAK1*.

Mutations in *IGSF9* (1/18, 6%) and *IGSF10* (4/18, 22%), members of the immunoglobulin superfamily, were found exclusively in GI-TNKLs. So far, no strong associations have been reported between immunoglobulin function and TNKs, except one recent study that showed a recurrent *IGSF10* mutation in familial gastric and colorectal cancer [15]. We expect that further in-depth studies can test the vulnerability of resident cells, such as mucosa epithelial cells and immune T cells, in the milieu of the GI-tract to *IGSF10* mutations.

Finally, we conducted direct Sanger sequencing to confirm the presence of mutations in *KCNB2*, *JAK3*, and *JAK1* (Supplementary Table 9 and Supplementary Appendix). In seven cases in which genomic DNA were available, nine mutations were validated (Supplementary Figure 12 and Supplementary Appendix).

In conclusion, we noted characteristic mutations of *KCNB2*, as well as *JAK3*, *JAK1*, and *IGSF10*, in GI-TNKLs. Although more comprehensive work is needed, the present findings provide some insights into understanding the physiological and pathological links between these genes and GI-TNKL genesis and into the potential for targeted therapy against tumor cells and the tumor microenvironment associated therewith.

Acknowledgements The study was supported by the Basic Science Research Program through the National Research Foundation of Korea (NRF), funded by the Ministry of Education (NRF-2015R1D1A1A09059399) (SOY). This work was supported by the Bio-Synergy Research Project (NRF-2017M3A9C4092978) of the Ministry of Science, ICT (SK).

Author contributions Contribution: SOY, SK, and GL conceived and designed the study, analyzed data, and drafted the paper; SOY, SK, GL, and HJR performed most of the research, analyzed the data, and edited the paper; JWC, HK, WIY, ISY, and M-kS analyzed the data.

Compliance with ethical standards

Conflict of interest The authors declare that they have no conflict of interest.

Open Access This article is licensed under a Creative Commons Attribution 4.0 International License, which permits use, sharing, adaptation, distribution and reproduction in any medium or format, as long as you give appropriate credit to the original author(s) and the source, provide a link to the Creative Commons license, and indicate if changes were made. The images or other third party material in this article are included in the article's Creative Commons license, unless indicated otherwise in a credit line to the material. If material is not included in the article's Creative Commons license and your intended use is not permitted by statutory regulation or exceeds the permitted use, you will need to obtain permission directly from the copyright holder. To view a copy of this license, visit <http://creativecommons.org/licenses/by/4.0/>.

References

1. Swerdlow SHCE, Harris NL, Jaffe ES, Pileri SA, Stein H, Thiele J. WHO Classification of Tumours of Haematopoietic and Lymphoid Tissues—WHO Classification of Tumours, revised 4th ed, Vol. 2. International Agency for Research on Cancer; Lyon 2017.
2. Lewin KJ, Ranchod M, Dorfman RF. Lymphomas of the gastrointestinal tract: a study of 117 cases presenting with gastrointestinal disease. *Cancer*. 1978;42:693–707.
3. Roberti A, Dobay MP, Bisig B, Vallois D, Boéchat C, Lanitis E, et al. Type II enteropathy-associated T-cell lymphoma features a unique genomic profile with highly recurrent SETD2 alterations. *Nat Commun*. 2016;7:12602.
4. Vogalis F. Potassium channels in gastrointestinal smooth muscle. *J Auton Pharmacol*. 2000;20:207–19.
5. Hammadi M, Chopin V, Matifat F, Dhennin-Duthille I, Chasserand M, Sevestre H, et al. Human ether à-gogo K⁺ channel 1 (hEag1) regulates MDA-MB-231 breast cancer cell migration through Orail-dependent calcium entry. *J Cell Physiol*. 2012;227:3837–46.
6. Agarwal JR, Griesinger F, Stühmer W, Pardo LA. The potassium channel Ether a go-go is a novel prognostic factor with functional relevance in acute myeloid leukemia. *Mol Cancer*. 2010;9:18.
7. Masi A, Becchetti A, Restano-Cassulini R, Polvani S, Hofmann G, Buccoliero A, et al. hERG1 channels are overexpressed in glioblastoma multiforme and modulate VEGF secretion in glioblastoma cell lines. *Br J Cancer*. 2005;93:781.
8. Brevet M, Fucks D, Chatelain D, Regimbeau J-M, Delcenserie R, Sevestre H, et al. Deregulation of 2 potassium channels in pancreatic adenocarcinomas: implication of KV1. 3 gene promoter methylation. *Pancreas*. 2009;38:649–54.
9. Eil R, Vodnala SK, Clever D, Klebanoff CA, Sukumar M, Pan JH, et al. Ionic immune suppression within the tumour microenvironment limits T cell effector function. *Nature*. 2016;537:539.
10. O'Grady SM, Lee SY. Molecular diversity and function of voltage-gated (Kv) potassium channels in epithelial cells. *Int J Biochem Cell Biol*. 2005;37:1578–94.
11. Küçük C, Jiang B, Hu X, Zhang W, Chan JK, Xiao W, et al. Activating mutations of STAT5B and STAT3 in lymphomas derived from $\gamma\delta$ -T or NK cells. *Nat Commun*. 2015;6:6025.

12. Nairismägi M, Tan J, Lim J, Nagarajan S, Ng C, Rajasegaran V, et al. JAK-STAT and G-protein-coupled receptor signaling pathways are frequently altered in epitheliotropic intestinal T-cell lymphoma. *Leukemia*. 2016;30:1311.
13. Koo GC, Tan SY, Tang T, Poon SL, Allen GE, Tan L, et al. Janus kinase 3-activating mutations identified in natural killer/T-cell Lymphoma. *Cancer Discov*. 2012.
14. Nicolae A, Xi L, Pham TH, Pham T-A, Navarro W, Meeker HG, et al. Mutations in the JAK/STAT and RAS signaling pathways are common in intestinal T-cell lymphomas. *Leukemia*. 2016;30:2245–2247.
15. Thutkawkorapin J, Picelli S, Kontham V, Liu T, Nilsson D, Lindblom A. Exome sequencing in one family with gastric-and rectal cancer. *BMC Genet*. 2016;17:41.

Leukemia (2019) 33:1801–1805

<https://doi.org/10.1038/s41375-018-0322-7>

Chronic lymphocytic leukemia

Different time-dependent changes of risk for evolution in chronic lymphocytic leukemia with mutated or unmutated antigen B cell receptors

Theodoros Moysiadis¹ · Panagiotis Baliakas² · Davide Rossi³ · Mark Catherwood⁴ · Jonathan C. Strefford⁵ · Julio Delgado⁶ · Achilles Anagnostopoulos⁷ · Chrysoula Belessi⁸ · Niki Stavroyianni⁷ · Sarka Pospisilova⁹ · David Oscier¹⁰ · Gianluca Gaidano¹¹ · Elias Campo¹² · Richard Rosenquist^{2,13} · Paolo Ghia¹⁴ · Kostas Stamatopoulos^{1,2}

Received: 9 August 2018 / Revised: 25 October 2018 / Accepted: 29 October 2018 / Published online: 24 January 2019

© Springer Nature Limited 2019

To the Editor:

Chronic lymphocytic leukemia (CLL) displays remarkable clinical heterogeneity, likely attributed to the underlying

biological diversity [1]. This claim is supported by the fact that certain immunogenetic and/or genomic features identify subgroups of CLL patients with distinct prognosis and outcome [2–4]. Indeed, determination of the somatic hypermutation (SHM) status of the immunoglobulin heavy variable (IGHV) genes expressed by the clonotypic B cell receptor (BcR) and screening for aberrations of the *TP53* gene are nowadays considered essential for clinical decision making [5]. A cautionary note appears warranted when

Supplementary information The online version of this article (<https://doi.org/10.1038/s41375-018-0322-7>) contains supplementary material, which is available to authorized users.

✉ Kostas Stamatopoulos
kostas.stamatopoulos@gmail.com

¹ Institute of Applied Biosciences, Center for Research and Technology Hellas, Thessaloniki, Greece

² Department of Immunology, Genetics and Pathology, Science for Life Laboratory, Uppsala University, Uppsala, Sweden

³ Division of Hematology, Oncology Institute of Southern Switzerland, Bellinzona, Switzerland

⁴ Department of Hemato-Oncology, Belfast City Hospital, Belfast, UK

⁵ Cancer Genomics, Academic Unit of Cancer Sciences, Cancer Research UK Centre and Experimental Cancer Medicine Centre, Faculty of Medicine, University of Southampton, Southampton, UK

⁶ Hematology Department, Hospital Clinic, Barcelona, Spain

⁷ Hematology Department and HCT Unit, G. Papanicolaou Hospital, Thessaloniki, Greece

⁸ Hematology Department, Nikea General Hospital, Pireaus, Greece

⁹ Central European Institute of Technology, Masaryk University and University Hospital Brno, Brno, Czech Republic

¹⁰ Department of Haematology, Royal Bournemouth Hospital, Bournemouth, UK

¹¹ Division of Hematology, Department of Translational Medicine, Amedeo Avogadro University of Eastern Piedmont, Novara, Italy

¹² Hematopathology Section, Laboratory of Pathology, Hospital Clinic of Barcelona, University of Barcelona, IDIBAPS, Barcelona, Spain

¹³ Department of Molecular Medicine and Surgery, Karolinska Institutet, Stockholm, Sweden

¹⁴ Division of experimental Oncology, IRCCS Istituto Scientifico San Raffaele and Università Vita-Salute San Raffaele, Milan, Italy

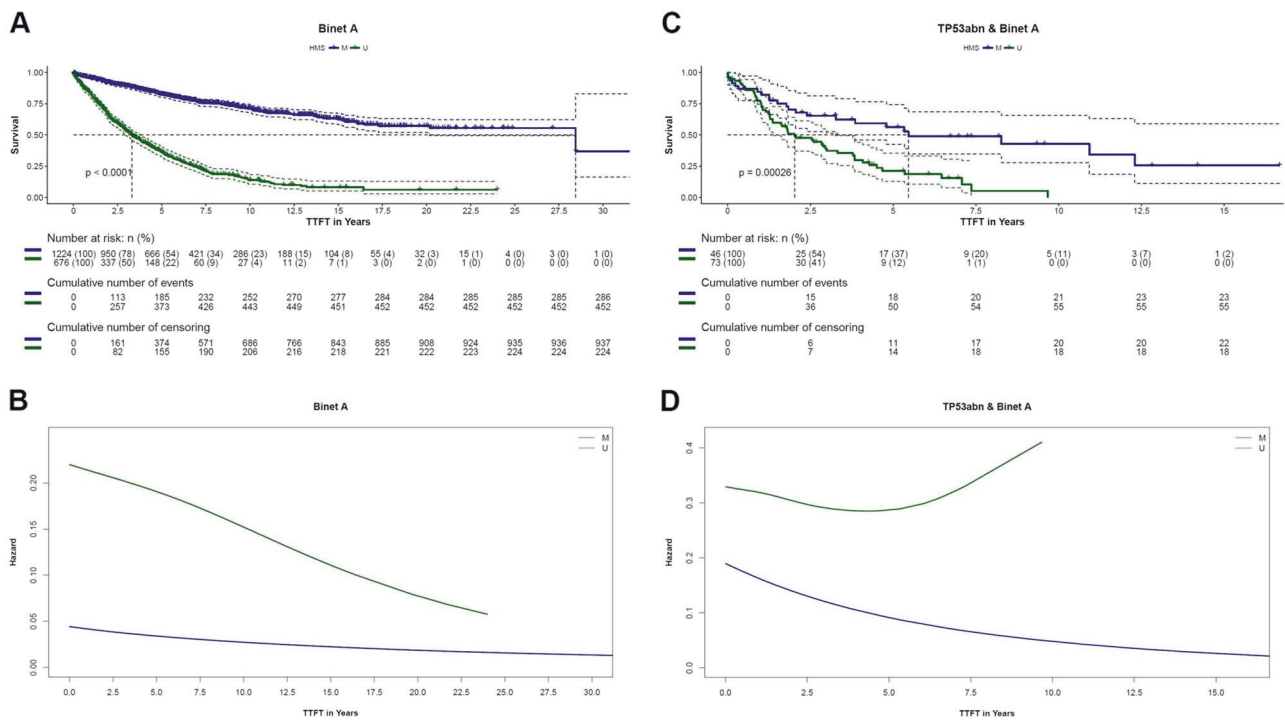


Fig. 1 Standard Kaplan–Meier survival plot and hazard plot for the entire cohort and the *TP53abn* patients. The hazard plot shows the estimated proportion of patients who received treatment for the first time in a defined time interval, given that they were still treatment-free at the start of this interval. The p -value corresponding to the log-rank test for the comparison of the survival distributions is displayed in the survival plot. The table including the number of patients at risk, and

the cumulative number of events/censoring, applies in both plots. For both subgroups, the survival curves (**a**, **c**) exhibited a similar behavior. When considering the hazard curves (**b**, **d**), M-CLL showed a gradual decrease in both subgroups, while U-CLL exhibited significant differences over-time with a constant decrease over-time in the entire cohort (**b**) and initial decrease until the fifth year and sudden increase for the *TP53abn* patients (**d**)

utilizing biomarkers, where the prognosis is usually assessed assuming stable predictability over the disease course; this hypothesis, however, is often unrealistic as it concerns genomic aberrations [6, 7]. Therefore, arguably, the prognostic power of a given biomarker may, instead, heavily depend on the time distance from diagnosis.

To address this issue we investigated in early-stage CLL patients the impact over-time of SHM within the IGHV genes, i.e., the segregation into mutated (M-CLL) and unmutated CLL (U-CLL), on the evolution of risk for CLL progression and need of treatment. Our analysis was based on hazard curves instead of Kaplan–Meier survival curves, which represent, respectively, the “instant” risk for the event at each time-point instead of the cumulative risk [8, 9].

Overall, 1900 early-stage, Binet A CLL patients from 10 European institutions diagnosed according to the 2008 iwCLL criteria [10] were included in this retrospective study (summary of patient characteristics: Supplemental Table 1). Ethical approval was granted by the local review committees and informed consent was collected according to the Helsinki Declaration.

Fluorescence in situ hybridization (FISH) was performed in 1476/1900 (77.7%) cases using probes for the 13q14, 11q22, 17p13 regions and trisomy 12; results were

interpreted following Döhner’s hierarchical model [11]. Genes analyzed for mutations included *TP53* (exons 4–10, $n = 1186/1900$, 62.4%), *SF3B1* (exons 14–16, $n = 1166/1900$, 61.4%) and *NOTCH1* (entire exon 34 or targeted analysis for del17544–45/p.P2514Rfs*4, $n = 1691/1900$, 89%). Sequence analysis of IGHV/IGHD/IGHJ rearrangements was performed in all cases as described [12]. All FISH, gene mutation screens and IG gene sequencing studies were performed once before the administration of any treatment; in 1702/1900 (90%) cases, these tests were performed within the first year from diagnosis.

In order to assess the risk for disease progression, we evaluated the time-to-first-treatment from diagnosis within different genomic subgroups, with risk evolution over-time represented by a hazard curve. Smoothed estimates of the hazard curve were computed separately for M-CLL and U-CLL, based on a non-parametric methodology (“bshazard” package) [13].

To compare the evolution pattern of hazard curves for each subgroup, we investigated over-time both their differences and ratios. Years 5, 10, and 15 after diagnosis were considered as landmark time-points for over-time comparison. The distributions of hazard differences were statistically compared between consecutive 5-year intervals to

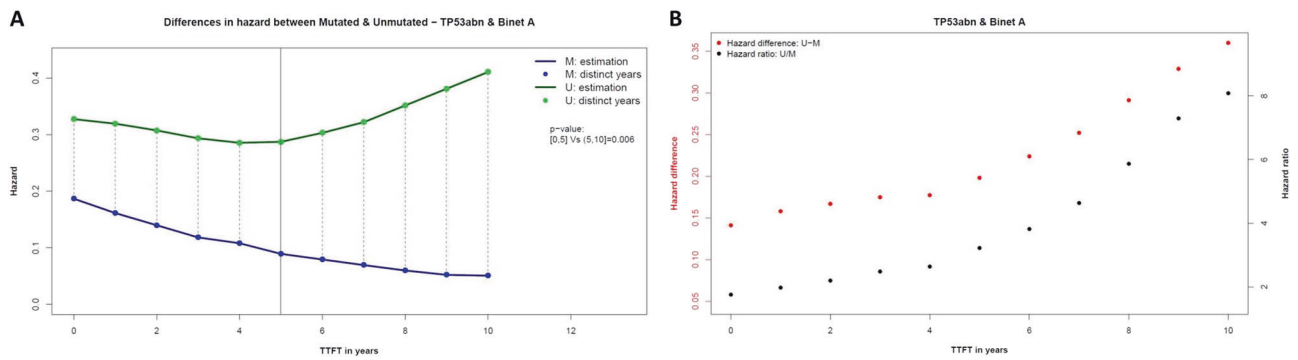


Fig. 2 Hazard plot and evolution of hazard differences/ratios for the *TP53abn* patients. **a** The hazard plot shows the estimated proportion of patients who received treatment for the first time in a defined time interval, given that they were still treatment-free at the start of this interval. The hazard differences between the M-CLL and U-CLL curves are represented by vertical dashed lines. The *p*-value of the

assess the evolution over-time (trend) of the distance between the hazard curves of the M-CLL and U-CLL patients. *p*-values less than 0.05 might indicate convergence or divergence of the curves within consecutive 5-year intervals. Regarding the hazard ratios for M-CLL and U-CLL, the proportional hazards assumption was checked. Moreover, a method able to identify the break points in the hazard was applied (“RPEXE.RPEXT” package) [14]. The analysis was performed with R. Details about the statistical methodology are provided in Supplemental Material.

Based on the SHM status, 1224 (64.4%) and 676 (35.6%) patients were classified as M-CLL and U-CLL, respectively. The over-time risk for evolution was evaluated with SHM status as a reference using hazard plots in: (i) the entire cohort, (ii) cases with *TP53* aberrations (*TP53abn*: del [17p] and/or *TP53* mutations), (iii) cases carrying del[11q] with no *TP53abn* (del[11q], non *TP53abn*), (iv) cases carrying +12 with no *TP53abn* (+12, non *TP53abn*), (v) cases carrying isolated del[13q] or normal FISH according to the Döhner model [11] (del[13q]/normal FISH), (vi) *NOTCH1* mutations, and (vii) *SF3B1* mutations.

In both the entire cohort and *TP53abn* patients, M-CLL exhibited gradual risk decrease over-time (Figs. 1b, d). In contrast, in U-CLL, a constant decrease was observed in the entire cohort, while in *TP53abn* cases the hazard curve initially decreased until the fifth year and then started to increase, indicating intensification of the risk for progression after the fifth year (Figs. 1b, d). Notably, the survival plots (Figs. 1a, c) failed to highlight any difference regarding the over-time risk between M-CLL and U-CLL and exhibited a similar behavior with slowly increasing distance between the M-CLL and U-CLL survival curves over-time.

In the remaining cases (Supplemental Fig. 1–5), the M-CLL hazard curve slowly decreased except for del[11q] patients. In U-CLL, there was a wide range for hazard

comparison within consecutive 5-year intervals of the distributions of hazard differences between M-CLL and U-CLL is also displayed. **b** The evolution of the hazard difference, U-CLL–M-CLL, with its scale displayed in the left vertical axis in red, and the evolution of the hazard ratio, U-CLL/M-CLL, with its scale displayed in the right vertical axis in black, are simultaneously displayed for the *TP53abn* patients

evolution: from decrease, such as for patients with del[13q]/normal FISH), del[11q], and *NOTCH1* mutations; to almost stable hazard over-time (*SF3B1* mutant patients). Interestingly, +12 patients showed a risk evolution similar to cases with *TP53abn*.

Regarding the distribution of hazard differences, significant differences were found in the entire cohort between M-CLL and U-CLL in all consecutive pairs of 5-year intervals with $p_{[0,5]Vs(5,10)} = 0.006$, $p_{(5,10)Vs(10,15)} = 0.009$, and $p_{(10,15)Vs(15,20)} = 0.009$ (Supplemental Figure 7A) reflecting a statistically significant decrease of the distance between the two hazard curves in all pairwise comparisons. The same evolution rule was followed by the del[13q]/normal-FISH patients as well as patients carrying del[11q] or *NOTCH1* mutations (Supplemental Figures 7D, 7B, 7E). For patients with *SF3B1* mutations, the distance between the two curves remained almost stable, $p_{[0,5]Vs(5,10)} = 0.465$ (Supplemental Figure 7F). In sharp contrast, within *TP53abn* patients, the distance between the hazard curves for M-CLL and U-CLL increased significantly after the 5th year with $p_{[0,5]Vs(5,10)} = 0.006$ (Fig. 2a). Similarly, in +12 patients, the U-CLL hazard curve constantly increased from diagnosis, with $p_{[0,5]Vs(5,10)} = 0.006$ (Supplemental Figure 7C).

Next, we tested the proportional hazards assumption (see Supplemental Table 2, Supplemental Figure 9) to test whether the hazard ratio between an U-CLL and an M-CLL patient depended on time. The assumption was rejected only for the *TP53abn* patients (*p*-value = 0.045), reflecting the great variation observed with hazard ratios ranging from 1.75 to 8.09.

We then introduced a novel tool to visualize the comparison of risk evolution between M-CLL and U-CLL patients, per subgroup, in terms of both the hazard differences and ratios. A characteristic example concerns *TP53abn* patients (Fig. 2b), where the hazard ratio of U-CLL to M-CLL increased linearly before and

exponentially after the 5th year. Moreover, amongst *TP53*abn cases, both the differences and the ratios exhibited the most pronounced change of all the subgroups considered with ranges 0.22 and 6.33, respectively. *TP53*abn and +12 patients (Supplemental Figure 8C) were the only subgroups where both the differences and the ratios increased monotonically over-time, reflecting the divergence of the hazard curves. By applying piecewise exponential distribution no breakpoints were observed.

The concept of hazard curves [15] has not been yet explored in CLL. The principal advantage of a hazard curve compared to the standard Kaplan–Meier survival curve is that it represents the “instant” risk for the event of interest at each time-point, instead of the cumulative risk until that point. This might prove important in CLL, where, typically, the prognostic power of any biomarker is assumed stable over the disease course, although this is often unrealistic concerning genomic aberrations. Hence, it is crucial to evaluate the temporal effect on the factors’ prognostic power regarding CLL progression.

Our approach was grounded on the fundamental segregation of CLL patients into M-CLL and U-CLL, since the SHM status remains stable over-time; [1] furthermore, M-CLL and U-CLL have distinct biological background underlying distinct clonal behavior and eventual outcome [1, 12]. Within each subgroup we assessed how time distance from diagnosis impacted the prognostic power of several biomarkers on CLL progression. Taking a step further, we proposed a new method to statistically evaluate the differences in risk evolution between these patient groups.

In M-CLL, the risk for disease evolution was rather homogeneous across different genomic subgroups, tending to gradually decrease over-time. In contrast, within U-CLL the pattern of over-time risk evolution was remarkably heterogeneous, greatly affected by the genomic background of the malignant clone. In particular, *TP53*abn cases exhibited a significant increase of disease evolution especially after the 5th year from diagnosis (further highlighted by the rejection of the proportional hazards assumption). A similar pattern was observed in +12 cases. A possible explanation for the hazard increase amongst U-CLL cases with *TP53*abn and +12 may relate to either the expansion of the clonal size over-time or the acquisition of extra genomic abnormalities, reflecting potential genomic instability.

In conclusion, differential patterns of risk evolution for disease progression in M-CLL versus U-CLL support the notion that the SHM status represents more than a simple prognostic/predictive marker, and that segregation of CLL patients based on SHM might aid to detect important time effects on risk evolution within genomic subgroups of CLL patients. Moreover, they imply that specific genomic

abnormalities may be linked to differential risk for disease progression over-time, while their prognostic impact may be modulated with the time elapsing from the initial diagnosis. This new methodology for evaluating and visualizing the over-time risk for disease evolution in CLL is easy to apply and can be generalized to cover the case of scoring systems where the number of categories compared is more than two, arguably also in other disease contexts.

Acknowledgements This project has received funding from the European Union’s Horizon 2020 (EU H2020) research and innovation programme under the Marie Skłodowska-Curie grant agreement No 702714 CLLassify; the EU H2020 project AEGLE; the EU H2020 project MEDGENET; the Swedish Cancer Society, the Swedish Research Council, Knut and Alice Wallenberg Foundation, Karolinska Institutet, Stockholm, the Lion’s Cancer Research Foundation, Uppsala, the Marcus Borgström Foundation and Selander’s Foundation, Uppsala; CEITEC MEYS CR project LQ1601; EC is supported by grants from Instituto de Salud Carlos III (PMP15/00007, CIBER-ONC and ERA-NET TRANSCAN initiative (TRS-2015-00000143) AC15/00028.

Compliance with ethical standards

Conflict of interest KS and PG received research support from Janssen Pharmaceuticals, Gilead Sciences, Novartis SA, Abbvie and Roche Hellas. The remaining authors declare that they have no conflict of interest.

Publisher’s note: Springer Nature remains neutral with regard to jurisdictional claims in published maps and institutional affiliations.

References

- Fabbri G, Dalla-Favera R. The molecular pathogenesis of chronic lymphocytic leukaemia. *Nat Rev Cancer*. 2016;16:145–62.
- Baliakas P, Hadzidimitriou A, Sutton LA, Minga E, Agathangelidis A, Nichelatti M, et al. Clinical effect of stereotyped B-cell receptor immunoglobulins in chronic lymphocytic leukaemia: a retrospective multicentre study. *Lancet Haematol*. 2014;1:e74–84.
- Baliakas P, Hadzidimitriou A, Sutton LA, Rossi D, Minga E, Villamor N, et al. Recurrent mutations refine prognosis in chronic lymphocytic leukemia. *Leukemia*. 2015;29:329–36.
- Rossi D, Rasi S, Spina V, Bruscaggin A, Monti S, Ciardullo C, et al. Integrated mutational and cytogenetic analysis identifies new prognostic subgroups in chronic lymphocytic leukemia. *Blood*. 2013;121:1403–12.
- Hallek M, Cheson BD, Catovsky D, Caligaris-Cappio F, Dighiero G, Dohner H, et al. iwCLL guidelines for diagnosis, indications for treatment, response assessment, and supportive management of chronic lymphocytic leukemia. *Blood*. 2018;131:2745–60.
- Ljungstrom V, Cortese D, Young E, Pandzic T, Mansouri L, Plevova K, et al. Whole-exome sequencing in relapsing chronic lymphocytic leukemia: clinical impact of recurrent RPS15 mutations. *Blood*. 2016;127:1007–16.
- Sutton LA, Rosenquist R. The complex interplay between cell-intrinsic and cell-extrinsic factors driving the evolution of chronic lymphocytic leukemia. *Semin Cancer Biol*. 2015;34:22–35.
- Collett D. Modelling survival data in medical research. 3rd ed. Chapman and Hall/CRC, New York; 2015.

9. Klein JP, Moeschberger ML. Survival analysis: techniques for censored and truncated data. 2nd ed, Springer-Verlag, New York; 2006.
10. Hallek M, Cheson BD, Catovsky D, Caligaris-Cappio F, Dighiero G, Dohner H, et al. Guidelines for the diagnosis and treatment of chronic lymphocytic leukemia: a report from the International Workshop on Chronic Lymphocytic Leukemia updating the National Cancer Institute-Working Group 1996 guidelines. *Blood*. 2008;111:5446–56.
11. Dohner H, Stilgenbauer S, Benner A, Leupolt E, Krober A, Bullinger L, et al. Genomic aberrations and survival in chronic lymphocytic leukemia. *N Engl J Med*. 2000;343:1910–6.
12. Baliakas P, Moysiadis T, Hadzidimitriou A, Xochelli A, Jeromin S, Agathangelidis A, et al. Tailored approaches grounded on immunogenetic features for refined prognostication in chronic lymphocytic leukemia. *Haematologica*. 2018. (Epub ahead of print).
13. Rebora P, Salim A, Reilly M. bshazard: a flexible tool for non-parametric smoothing of the hazard function. *R J*. 2014;6:9.
14. Han G, Schell MJ, Kim J. Improved survival modeling in cancer research using a reduced piecewise exponential approach. *Stat Med*. 2014;33:59–73.
15. Pfeilstocker M, Tuechler H, Sanz G, Schanz J, Garcia-Manero G, Sole F, et al. Time-dependent changes in mortality and transformation risk in MDS. *Blood*. 2016;128:902–10.

Leukemia (2019) 33:1805–1810

<https://doi.org/10.1038/s41375-018-0343-2>

Chronic myeloproliferative neoplasms

Azacitidine is effective for targeting leukemia-initiating cells in juvenile myelomonocytic leukemia

Christopher F. Krombholz¹ · Lorena Gallego-Villar¹ · Sushree S. Sahoo¹ · Pritam K. Panda¹ · Marc W. Wlodarski^{1,2} · Konrad Aumann³ · Mark Hartmann⁴ · Daniel B. Lipka⁴ · Michael Daskalakis⁴ · Christoph Plass^{2,4} · Charlotte M. Niemeyer^{1,2} · Miriam Erlacher^{1,2} · Christian Flotho^{1,2}

Received: 3 August 2018 / Revised: 15 October 2018 / Accepted: 24 October 2018 / Published online: 24 January 2019

© Springer Nature Limited 2019

To the Editor:

Juvenile myelomonocytic leukemia (JMML) is a life-threatening myeloproliferative neoplasm of early childhood [1] originating from multipotent hematopoietic stem/progenitor cells [2] that requires allogeneic hematopoietic stem cell transplantation (HSCT) in the majority of cases [3]. We and others have linked the clinical picture and prognosis of

JMML to differential DNA methylation patterns in leukemic cells [4–7]. A retrospective case series documented that treatment with the DNA methyltransferase-inhibiting agent azacitidine achieved complete clinical and molecular remissions in children diagnosed with JMML, suggesting superior therapeutic potential of this drug [8]. To generate a preclinical research model for JMML, we have previously established a xenotransplantation system of this leukemia in *Rag2^{-/-}γc^{-/-}* mice [9]. Transplantation of primary JMML cells resulted in stable xenologous engraftment, reproduced a characteristic JMML phenotype, and sustained serial transplantations for up to 1.5 years [9]. Here we used the xenotransplantation system to study if leukemia-initiating cells determine the aberrant DNA methylation profiles in JMML. We then investigated the antileukemic activity of azacitidine in JMML xenografts in comparison to the cytostatic agent, cytosine arabinoside (cytarabine). The latter is used for cytorreduction in JMML but lacks the ability to induce complete remissions [3].

Xenotransplantations were prepared by irradiating neonatal *Rag2^{-/-}γc^{-/-}* BALB/c mice sublethally with 2.5 Gy. Six hours later, 1×10^6 CD3-depleted JMML mononuclear cells suspended in 30 μl of phosphate-buffered saline were injected intrahepatically. Histopathological examination of experimental animals, isolation of human cells from murine organs, and evaluation of cell populations by flow cytometry were

These authors contributed equally: Miriam Erlacher, Christian Flotho

Supplementary information The online version of this article (<https://doi.org/10.1038/s41375-018-0343-2>) contains supplementary material, which is available to authorized users.

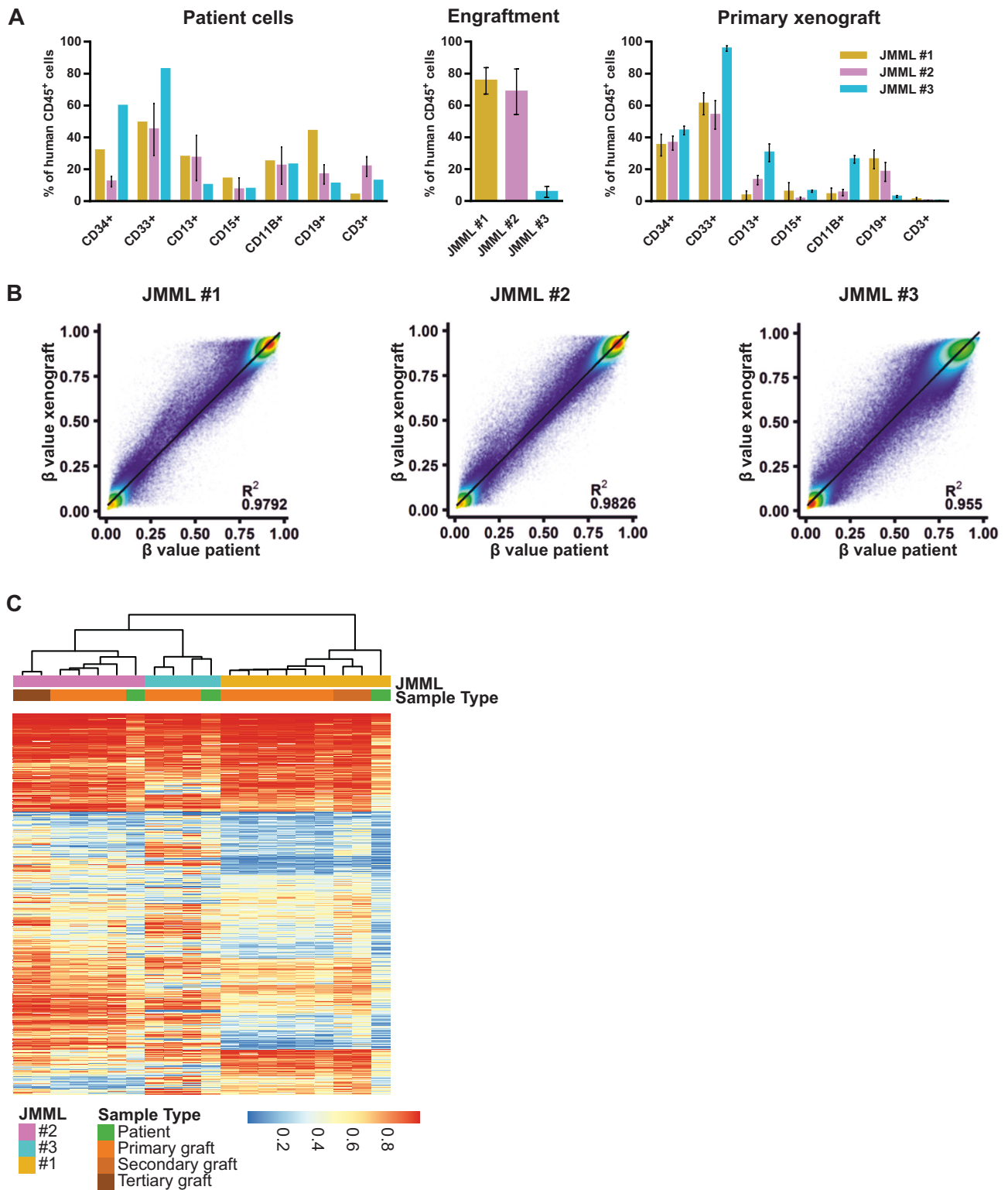
✉ Christian Flotho
christian.flotho@uniklinik-freiburg.de

¹ Division of Pediatric Hematology and Oncology, Department of Pediatrics and Adolescent Medicine, Medical Center, Faculty of Medicine, University of Freiburg, Freiburg, Germany

² German Cancer Consortium, Heidelberg, Germany

³ Department of Pathology, Medical Center, Faculty of Medicine, University of Freiburg, Freiburg, Germany

⁴ Division of Epigenomics and Cancer Risk Factors, German Cancer Research Center, Heidelberg, Germany



performed as previously described [9]. The experiments were approved by local authorities and complied with the German law for animal protection (Tierversuchsgesetz).

We first tested the hypothesis that the aberrant DNA methylation patterns observed in mature JMML cell progeny originate in leukemic stem cells. We used leukemia

cell samples isolated from spleens of three children with JMML (Supplementary Table 1) to initiate the disease in immunodeficient mice and compare DNA methylation profiles between the original patient samples and a total of 13 xenografts. Hematopoietic cell populations were assessed by flow cytometry in patient samples and corresponding

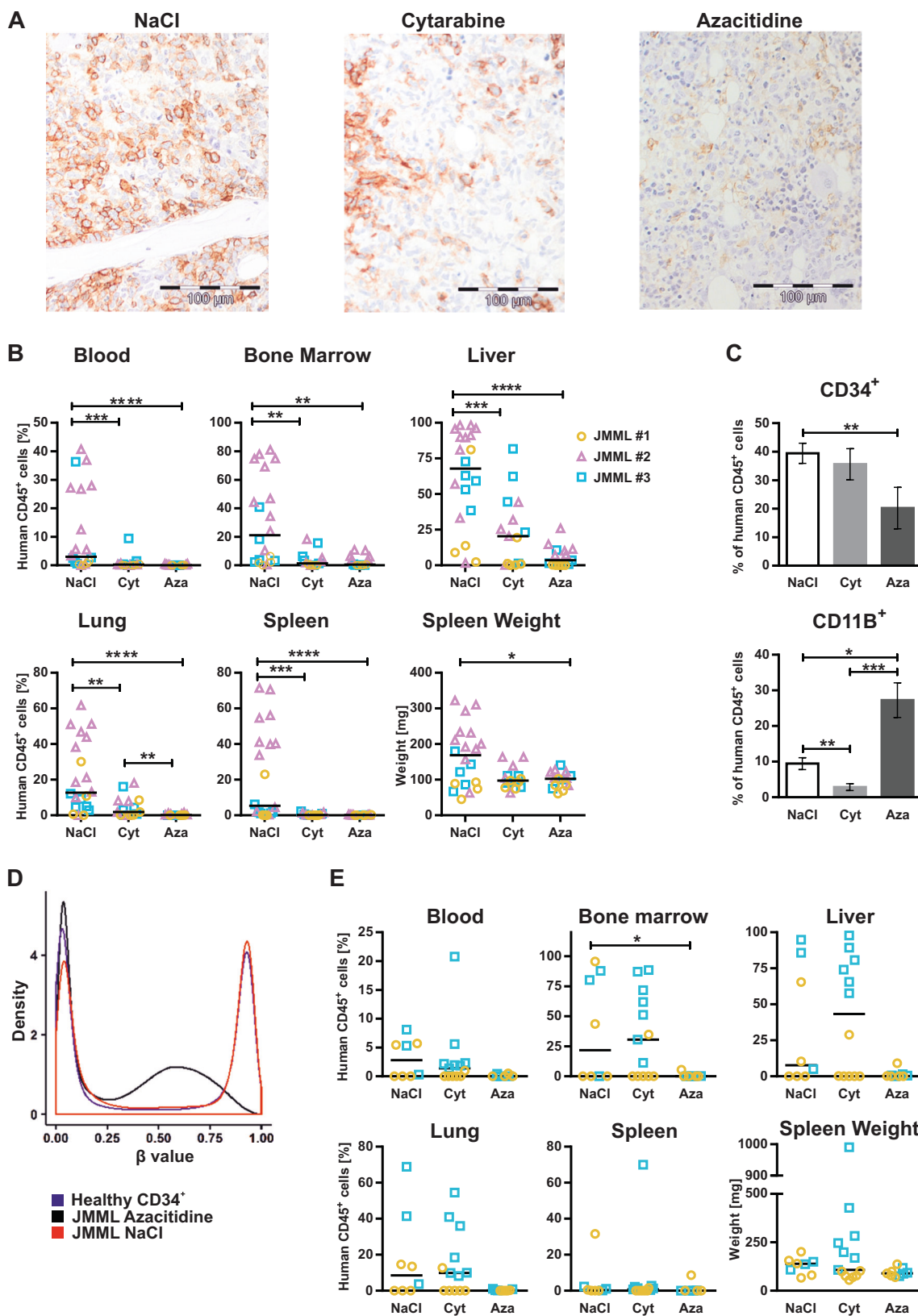
◀ **Fig. 1** DNA methylation patterns specific of each JMML case were recapitulated in xenotransplanted leukemias. **a** Left: hematopoietic cell populations in spleen cell samples of three patients with JMML. Center: engraftment levels of patient-derived xenografts (human CD45⁺ cells) in mouse bone marrow at 9–36 weeks after transplantation. Right: human hematopoietic cell populations among human CD45⁺ cells in mouse bone marrow. Values were determined by flow cytometry (1–2 aliquots per patient sample and 3–6 recipient mice per patient). Error bars represent standard errors. **b** Rainbow density plots of genome-wide CpG methylation in spleen cells of three patients with JMML (*X*-axis) and in human CD45⁺ cells extracted from bone marrow of xenotransplanted mice at 9–36 weeks after transplantation (*Y*-axis). DNA methylation was analyzed using Infinium Human Methylation 450K Bead Chip arrays (Illumina) as previously described [5]. The RnBeads software package was used for data normalization, filtering of single-nucleotide polymorphisms, removal of probes on sex chromosomes, and quantification. The plots were created with ggplot2 (version 2.2.1). JMML #1: 460,779 values are plotted (*X*-axis, average of two replicate samples run on separate arrays; *Y*-axis, average of cells from six recipient mice run on separate arrays). JMML #2: 460,697 values are plotted (*X*-axis, three replicate samples; *Y*-axis, four recipient mice). JMML #3: 460,182 values are plotted (*X*-axis, one sample; *Y*-axis, three recipient mice). The black line represents linear regression; R^2 , Pearson correlation coefficient. **c** Unsupervised hierarchical cluster analysis of genome-wide CpG methylation values in patient samples and xenotransplanted JMML cells (columns) using 5380 CpG sites (rows) with most variation of methylation between samples. CpG sites showing methylation changes during normal hematopoietic differentiation were excluded [5]. The chart includes the patient samples and primary xenografts described in **a**, **b**, two secondary xenografts of cells from patient #1 after serial retransplantation, and two tertiary xenografts of cells from patient #2. The dendrogram was constructed using heatmap.2 of the gplots package (version 3.0.1) with Manhattan distance and Ward linkage (ward.D2). Methylation values are color-coded from blue (0% methylation) to red (100% methylation)

xenografts, demonstrating similar leukemia immunophenotypes (Fig. 1a). Infinium 450K arrays were used for the genome-wide analysis of CpG methylation in primary JMML cells and xenografts. The technical reliability was assessed by processing three cell aliquots from the same clinical sample on separate arrays and was extraordinarily high (R^2 coefficients >0.99, Supplementary Figure 1). We found that the epigenomes of JMML cells were highly robust, with only minimal alteration induced by the xenotransplantation procedure (Fig. 1b). On average, 0.36% of 29,938 promoters and 0.44% of 29,765 intragenic regions were called as “differentially methylated” between source and xenograft (change in β -value >0.2, $p < 0.05$ adjusted for false discovery rate). These results provide compelling evidence that the DNA methylation patterns of JMML cells repopulating the murine bone marrow are programmed in the leukemia-initiating cell. The analysis was extended by combining the methylome data of the three patient samples and 13 primary xenografts with methylome data of two secondary xenografts derived from patient #1 after serial retransplantation, and two tertiary xenografts derived from patient #2. Unsupervised clustering of ~5000 CpG sites with most variable methylation in JMML resulted in a dendrogram where all xenotransplanted leukemias associated with their

original patient sample (Fig. 1c). Together, the data indicate that xenotransplanted JMML-initiating cells faithfully reproduce the epigenetic make-up of the original leukemia.

We next xenotransplanted 50 mice with JMML cells from the three patients (Supplementary Figure 2) and compared the effects of treatment with azacitidine 3 mg/kg/d or cytarabine 20 mg/kg/d on xenografted JMML (5 days on and 9 days off, two cycles). Stable body weight indicated that the treatment was generally tolerated well by the experimental animals (Supplementary Figure 3). Cytarabine and azacitidine led to mild anemia and moderate thrombocytopenia in the mice compared to mock treatment (Supplementary Figure 4). Azacitidine strongly reduced the level of infiltration by human JMML cells in all organs analyzed (Fig. 2a, b). The effect was most pronounced in spleen (human CD45⁺ fraction of all CD45⁺ cells, 0.2% ± 0.04% versus 22.5% ± 5.8% in mice injected with saline; $p < 0.0001$) and lung (0.4% ± 0.12% versus 21.6% ± 4.5%; $p < 0.0001$) but significant also in bone marrow and liver. The splenomegaly caused by xenotransplantation of cells from patients JMML#1 and JMML#2 reverted to near-normal under treatment with azacitidine. Treatment with cytarabine reduced the human cell infiltration in murine organs to a similar degree. Importantly, however, we noted that CD34⁺ stem/progenitor cells within the human leukemia population were substantially reduced in the murine bone marrow after treatment with azacitidine (20.2% ± 7.3% versus 39.4% ± 3.5% in mice injected with saline; $p < 0.01$) but not cytarabine (35.6% ± 6.11%) (Fig. 2c). The relative amount of human leukemic granulocytes (CD11⁺) increased after treatment with azacitidine (27.2% ± 4.9% vs 9.4% ± 1.7%; $p < 0.05$). Concordant effects on infiltrating human CD34⁺ cells were observed in other organs (Supplementary Figure 5). The results fit with the expected activity of cytarabine as a cytostatic agent but suggest a different antileukemic effect of azacitidine on JMML.

To examine the hypomethylating effect of azacitidine on JMML cells in vivo, we determined Infinium 450K array profiles of human CD45⁺ cells extracted from the bone marrow of five JMML xenograft mice after treatment with azacitidine, human CD45⁺ cells extracted from five mice after mock treatment, and human CD34⁺ cells from four healthy individuals. The methylation values ($N = 307,923$) showed a bimodal distribution in healthy human CD34⁺ cells and mock-treated JMML cells as expected (Fig. 2d), with the vast majority of CpG sites being either unmethylated or completely methylated. The JMML cell samples obtained after treatment with azacitidine displayed dramatic global DNA demethylation with a complete loss of fully methylated CpG sites (Fig. 2d). However, enrichment analyses of demethylated enhancers or promoters failed to point out cellular components or pathways that might be specifically derepressed by azacitidine.



We then tested if the reduction of leukemic stem/progenitor cells by azacitidine was functionally relevant. After treating JMML xenograft mice with two cycles of

azacitidine, cytarabine, or saline solution, the murine bone marrow was transplanted into secondary recipient mice to assess its capacity to reinitiate the leukemia. We found that

◀ **Fig. 2** Azacitidine reduced the burden of JMML in xenotransplanted mice, depleted immature leukemic stem/progenitor cells, and impaired the leukemia-initiating capacity of JMML cells. Treatment consisted of intraperitoneal administration on five consecutive days of azacitidine 3 mg/kg/d (15 mice), cytarabine 20 mg/kg/d (15 mice), or 0.9% sodium chloride (20 mice). Azacitidine and cytarabine were dissolved in ice-cold water (0.5 mg/ml) and phosphate-buffered saline (3 mg/ml), respectively. Two cycles of 5-day treatment and 9-day rest were administered in weeks 8 and 10. The mice were sacrificed and analyzed at 12 weeks after transplantation. **a** Immunohistochemistry of bone marrow sections after two cycles of treatment with saline solution (left), cytarabine (middle), or azacitidine (right). Murine cells appear blue whilst human CD45⁺ cells stain brown. **b** The leukemic infiltration of different organs was assessed by flow cytometry measuring the ratio of human among all CD45⁺ cells in blood, bone marrow, liver, lung, and spleen. Single cell suspensions were prepared from liver and lung by passing chopped tissue through 70 μm strainers after incubation with collagenase and DNase. The bottom right panel shows the spleen weight of experimental animals after treatment. Xenografts are color-coded by patient of origin (orange circles, JMML #1; pink triangles, JMML #2; blue squares, JMML #3). The horizontal lines indicate median values. **c** Human JMML cell subpopulations CD34⁺ and CD11B⁺ in murine bone marrow after treatment as determined by flow cytometry. Bars represent mean values and standard errors. **d** Genome-wide methylation analysis using Infinium 450K arrays was performed using human CD45⁺ cells purified from bone marrow of five mice treated with azacitidine and five mice treated with saline solution. In addition, four methylomes of human CD34⁺ bone marrow cells obtained from healthy adults were included in the analysis. Average values per CpG site were calculated within each group of samples. After filtering CpG sites for missing values in at least one group, location close to polymorphisms, or known variable methylation in hematopoietic cells, 307,923 sites were used. The density plot illustrates the distribution of CpG dinucleotide methylation (β -values) in the three groups. **e** Treatment with saline solution, cytarabine, or azacitidine was administered as described to *Rag2*^{-/-}*γc*^{-/-} mice xenotransplanted with JMML cells from patient #1 or #3 (saline solution, eight mice; cytarabine, ten mice; azacitidine, ten mice). Bone marrow was harvested at 12 weeks after transplantation, and 2×10^6 whole bone marrow cells were transplanted into secondary recipients (cells from saline-treated primary animals, eight mice; cells from cytarabine-treated primary animals, 13 mice; cells from azacitidine-treated primary animals, nine mice). The 30 secondary recipient mice were sacrificed at 20 weeks after transplantation and analyzed by flow cytometry. The leukemic infiltration (percentage of human CD45⁺ among all CD45⁺ cells) of different organs is shown. The bottom right panel shows the spleen weight of secondary recipient mice. Xenografts are color-coded by patient of origin (orange circles, JMML #1; blue squares, JMML #3). The horizontal lines indicate median values. NaCl sodium chloride, Cyt cytarabine, Aza azacitidine. Significance levels (Mann–Whitney test): * $p < 0.05$, ** $p < 0.01$, *** $p < 0.001$, **** $p < 0.0001$

JMML cells obtained from azacitidine-treated primary recipients were engrafted in only one of nine secondary recipient mice at 30 weeks after retransplantation (defined as >0.5% human CD45⁺ cells in the bone marrow) (Fig. 2e, Supplementary Table 2). By contrast, JMML cells from primary recipients treated with cytarabine engrafted in eight of 13 secondary mice ($p = 0.03$, Fisher exact test). Of note, there was no difference in secondary engraftment between JMML cells treated with cytarabine and those treated with saline. Collectively, the retransplantation experiments provide in vivo evidence that azacitidine is more effective than

cytarabine for targeting leukemia-initiating cells in JMML, despite the structural similarity of both compounds as cytosine nucleoside analogs.

Low-dose azacitidine has shown promising clinical activity in children diagnosed with JMML [8], corresponding to its potent antileukemic effect in the xenotransplantation model. Consistent with our repopulation assays, azacitidine was reported to support remissions for up to 11 months in patients [8]. However, we do not expect monotherapy with azacitidine to be eventually curative for JMML, similar to observations for other malignant myeloid disorders [10]. An attractive perspective would be the use of azacitidine before HSCT with the aim of reducing both the relapse rate and the risks involved with the transplant procedure. Whether this concept works out in reality is open. The ongoing industry-sponsored Pediatric Investigation Plan for the prospective evaluation of azacitidine in children with JMML before HSCT (EudraCT number 2014-002388-13, ClinicalTrials.gov identifier NCT02447666) will help answer these questions.

The precise mechanism of the antineoplastic activity of azacitidine is incompletely understood. The methylome data of xenotransplanted JMML cells exposed to azacitidine demonstrate that this substance exerts effective inhibition of DNA methyltransferases in JMML cells and shifts the widespread CpG island hypermethylation back toward normal levels. However, the precise genes where this effect is relevant have yet to be defined. In addition, azacitidine induced genome-wide hypomethylation at sites where cytosine methylation is physiologic. Previous landmark studies have highlighted the profound consequences of demethylating repetitive DNA elements and long terminal repeats, resulting in activation of endogenous retroviral double-stranded RNA sequences [11, 12] and production of irregular RNA transcripts [13]. A concept with increasing popularity in the field stipulates that the expression of neoantigens and production of aberrant peptides following treatment with DNA-hypomethylating agents enhances the autologous anti-tumor immune response [14, 15]. It is an interesting discussion point in this regard that azacitidine was highly effective against JMML in our xenotransplantation model even though the host animals lacked functional T, B, or NK cells.

Acknowledgements This work was supported by the German Research Foundation (FOR2036 ER599/3-2 to M.E., CRC992-C05 and SPP1463 FL345/4-2 to C.F.).

Compliance with ethical standards

Conflict of interest The authors declare that they have no conflict of interest.

Publisher's note: Springer Nature remains neutral with regard to jurisdictional claims in published maps and institutional affiliations.

References

- Niemeyer CM, Locatelli F. Chronic myeloproliferative disorders. In: Pui CH, editor. *Childhood leukemias*. 3rd ed. New York: Cambridge University Press; 2012. p. 444–502.
- Flotho C, Valcamonica S, Mach-Pascual S, Schmahl G, Corral L, Ritterbach J, et al. RAS mutations and clonality analysis in children with juvenile myelomonocytic leukemia (JMML). *Leukemia*. 1999;13:32–37.
- Locatelli F, Niemeyer CM. How I treat juvenile myelomonocytic leukemia. *Blood*. 2015;125:1083–90.
- Olk-Batz C, Poetsch AR, Nöllke P, Claus R, Zucknick M, Sandrock I, et al. Aberrant DNA methylation characterizes juvenile myelomonocytic leukemia (JMML) with poor outcome. *Blood*. 2011;117:4871–80.
- Lipka DB, Witte T, Toth R, Yang J, Wiesenfarth M, Nöllke P, et al. RAS-pathway mutation patterns define epigenetic subclasses in juvenile myelomonocytic leukemia. *Nat Commun*. 2017;8:2126.
- Stieglitz E, Mazor T, Olshen AB, Geng H, Gelston LC, Akutagawa J, et al. Genome-wide DNA methylation is predictive of outcome in juvenile myelomonocytic leukemia. *Nat Commun*. 2017;8:2127.
- Murakami N, Okuno Y, Yoshida K, Shiraiishi Y, Nagae G, Suzuki K, et al. Integrated molecular profiling of juvenile myelomonocytic leukemia. *Blood*. 2018;131:1576–86.
- Cseh A, Niemeyer CM, Yoshimi A, Dworzak M, Hasle H, van den Heuvel-Eibrink MM, et al. Bridging to transplant with azacitidine in juvenile myelomonocytic leukemia: a retrospective analysis of the EWOG-MDS study group. *Blood*. 2015;125:2311–3.
- Krombholz CF, Aumann K, Kollek M, Bertele D, Fluhr S, Kunze M, et al. Long-term serial xenotransplantation of juvenile myelomonocytic leukemia recapitulates human disease in Rag2-/- gammadelta-/- mice. *Haematologica*. 2016;101:597–606.
- Flotho C, Sommer S, Lübbert M. DNA-hypomethylating agents as epigenetic therapy before and after allogeneic hematopoietic stem cell transplantation in myelodysplastic syndromes and juvenile myelomonocytic leukemia. *Semin Cancer Biol*. 2018;51:68–79.
- Roulois D, Loo YH, Singhania R, Wang Y, Danesh A, Shen SY, et al. DNA-demethylating agents target colorectal cancer cells by inducing viral mimicry by endogenous transcripts. *Cell*. 2015;162:961–73.
- Chiappinelli KB, Strissel PL, Desrichard A, Li H, Henke C, Akman B, et al. Inhibiting DNA methylation causes an interferon response in cancer via dsRNA including endogenous retroviruses. *Cell*. 2015;162:974–86.
- Brocks D, Schmidt CR, Daskalakis M, Jang HS, Shah NM, Li D, et al. DNMT and HDAC inhibitors induce cryptic transcription start sites encoded in long terminal repeats. *Nat Genet*. 2017;49:1052–60.
- Goodyear O, Agathangelou A, Novitzky-Basso I, Siddique S, McSkeane T, Ryan G, et al. Induction of a CD8+T-cell response to the MAGE cancer testis antigen by combined treatment with azacitidine and sodium valproate in patients with acute myeloid leukemia and myelodysplasia. *Blood*. 2010;116:1908–18.
- Li H, Chiappinelli KB, Guzzetta AA, Easwaran H, Yen RW, Vatapalli R, et al. Immune regulation by low doses of the DNA methyltransferase inhibitor 5-azacitidine in common human epithelial cancers. *Oncotarget*. 2014;5:587–98.

Leukemia (2019) 33:1810–1814

<https://doi.org/10.1038/s41375-018-0337-0>

Chronic myelogenous leukemia

Nilotinib-induced metabolic dysfunction: insights from a translational study using in vitro adipocyte models and patient cohorts

Soban Sadiq¹ · Euan Owen¹ · Terry Foster¹ · Katy Knight² · Lihui Wang² · Munir Pirmohamed¹ · Richard E. Clark³ · Sudeep Pushpakom¹

Received: 29 June 2018 / Revised: 3 November 2018 / Accepted: 20 November 2018 / Published online: 28 January 2019

© Springer Nature Limited 2019. This article is published with open access

Supplementary information The online version of this article (<https://doi.org/10.1038/s41375-018-0337-0>) contains supplementary material, which is available to authorized users.

✉ Sudeep Pushpakom
sudeep@liverpool.ac.uk

¹ Molecular and Clinical Pharmacology, University of Liverpool, Liverpool, United Kingdom

² Royal Liverpool and Broadgreen University Hospitals NHS Trust, Liverpool, United Kingdom

³ Institute of Translational Medicine, University of Liverpool, Liverpool, United Kingdom

To the Editor:

Nilotinib, a second-generation tyrosine kinase inhibitor (TKI), has been described to be a superior drug in the frontline treatment of patients with Philadelphia chromosome-positive (Ph+) chronic myeloid leukemia (CML) [1]. However, with more mature follow-up, it has become clear that nilotinib is associated with impaired glucose and lipid metabolism [2–4] and an excess in arterial thrombotic events in comparison to imatinib [5]. The 5-year safety update of the ENESTnd trial [3] provided further confirmation; it reported significant elevations in fasting glucose and serum lipids and an increased

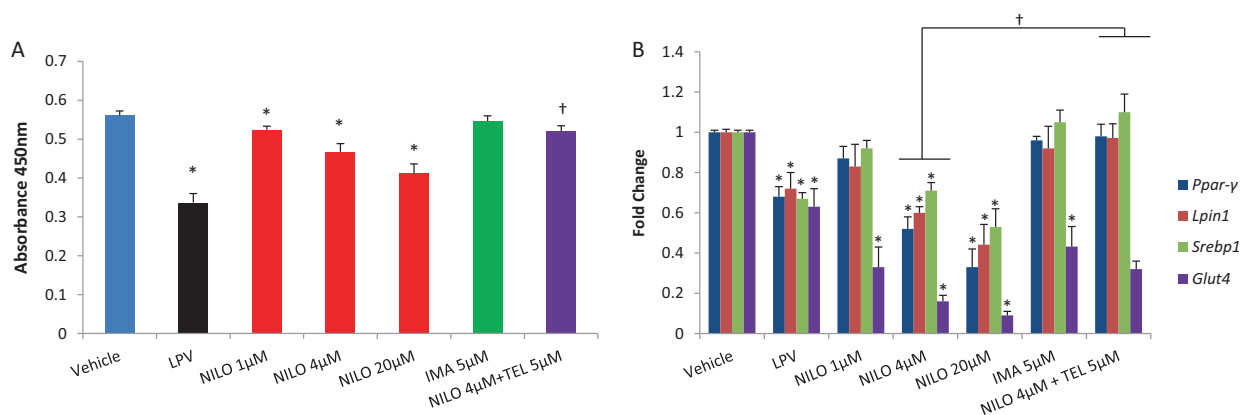


Fig. 1 Effect of nilotinib (with or without telmisartan) and imatinib on adipocyte lipid accumulation and mRNA expression of *Pparγ*, *Lpin1*, *Srebp1* and *Glut4* in differentiating 3T3-F442A adipocytes. **1A** Lipid droplets were stained with Oil Red O on day 10 following treatment with respective drugs/vehicle. Lipid bound Oil Red O was extracted with isopropyl alcohol and absorbance was measured at 450 nm. **1B** Gene expression of *Pparγ*, *Lpin1*, *Srebp1* and *Glut4* were assessed by real-time PCR using Taqman assays-on-demand gene expression assays (Life Technologies) on a 7900HT Fast Real-Time PCR system (Life Technologies). *Hprt* was used as an endogenous control. The

mRNA expression was calculated using the comparative Ct method according to the manufacturer's protocol and the fold change for the gene of interest was expressed as $2^{-\Delta\Delta CT}$. Telmisartan was co-incubated with only one concentration of nilotinib (4 µM). Lopinavir (LPV), an anti-HIV drug, was used as a positive control. All experiments were repeated three times in triplicate. Statistical analyses were conducted by one-way ANOVA with Dunnett's Test. Data represent Mean ± SD; $p \leq 0.05$. *Vehicle vs NILO/LPV/IMA; †NILO4µM vs NILO4µM + TEL5µM. NILO: nilotinib, IMA: imatinib, TEL: telmisartan, LPV: lopinavir, *Hprt*: Hypoxanthinephosphoribosyltransferase

incidence of cardiovascular events in nilotinib-treated patients as opposed to imatinib [3].

Adipose tissue is an important determinant of whole body glucose and lipid homeostasis [6], and adipocyte dysregulation is known to result in various metabolic abnormalities [7]. Accumulation of drugs in adipose tissue could result in adipocyte toxicity; we have shown that anti-HIV drugs cause adipocyte toxicity leading to insulin resistance and the development of cardiometabolic disease in HIV-positive individuals [8]. We hypothesised that nilotinib could cause adipocyte toxicity leading to various metabolic adverse effects in CML patients; here we have undertaken a translational study using in vitro–in vivo models to characterise this. We have also tested telmisartan, an angiotensin receptor blocker (ARB) and antihypertensive with beneficial metabolic effects [9], as a potential therapeutic strategy to reduce nilotinib-induced metabolic toxicity in vitro.

A chronic in vitro toxicity model as previously described [8], consisting of 3T3-F442A murine preadipocyte cells, was used to investigate the effect of nilotinib and imatinib on adipocytes. Briefly, differentiating adipocytes were incubated with either nilotinib (with or without telmisartan) or imatinib 48 h post-initiation of differentiation, and drug treatment was continued every 48 hours over a period of 10 days to mimic the chronic dosing schedule in CML patients. Nilotinib (1–4 µM) and imatinib (5 µM) were used within their therapeutic range; given the lipophilicity of nilotinib, we also assessed a hypothetical higher nilotinib concentration (20 µM) assuming adipose tissue accumulation following chronic drug treatment. Lopinavir, an anti-HIV drug known to cause adipocyte toxicity and metabolic

disturbances [8], was used as positive control. We have only investigated these two TKIs in the current study. Statistical analyses were conducted by one-way ANOVA with Dunnett's Test. All in vitro experiments were repeated three times in triplicate. A p value ≤ 0.05 was considered significant.

We investigated whether nilotinib and/or imatinib (0.01–100 µM) caused cytotoxicity in both undifferentiated and differentiating adipocytes using the MTT assay. Neither nilotinib nor imatinib reduced cell viability in these cell types at clinically relevant concentrations (Supplementary Figure 1). We hypothesised that nilotinib may interfere with adipocyte lipid accumulation and alter mRNA levels of key adipogenic regulatory genes (*Pparγ*, *Lpin1*, *Srebp1*). Lipid accumulation in differentiated adipocytes was assessed on day 10 using Oil Red O staining [8] and gene expression was assessed by Real-Time PCR using Taqman assays (Life Technologies). Nilotinib (4 µM: 0.46 absorbance units ± 0.02, $p = 0.001$), but not imatinib, caused dose-dependent reduction in adipocyte lipid accumulation when compared with the vehicle (0.56 ± 0.01) (Fig. 1A; also see Supplementary Figure 2). Reduced lipid droplet formation observed with nilotinib may suggest the inability of adipose tissue to store lipids; this will result in the ectopic accumulation of fat in the liver and skeletal muscle leading to the development of insulin resistance [10]. Nilotinib, but not imatinib, also resulted in dose-dependent downregulation of all three adipogenic regulatory genes, with the effect evident at therapeutic concentrations (4 µM nilotinib: *Ppar-γ*: 48% downregulation, *Lpin1*: 40% downregulation, *Srebp1*: 29% downregulation; all $p < 0.05$; Fig. 1B). *PPARγ* is a master regulator of adipogenesis and mediates adipogenic gene expression and insulin sensitivity [11]; *lipin1*, a gene that

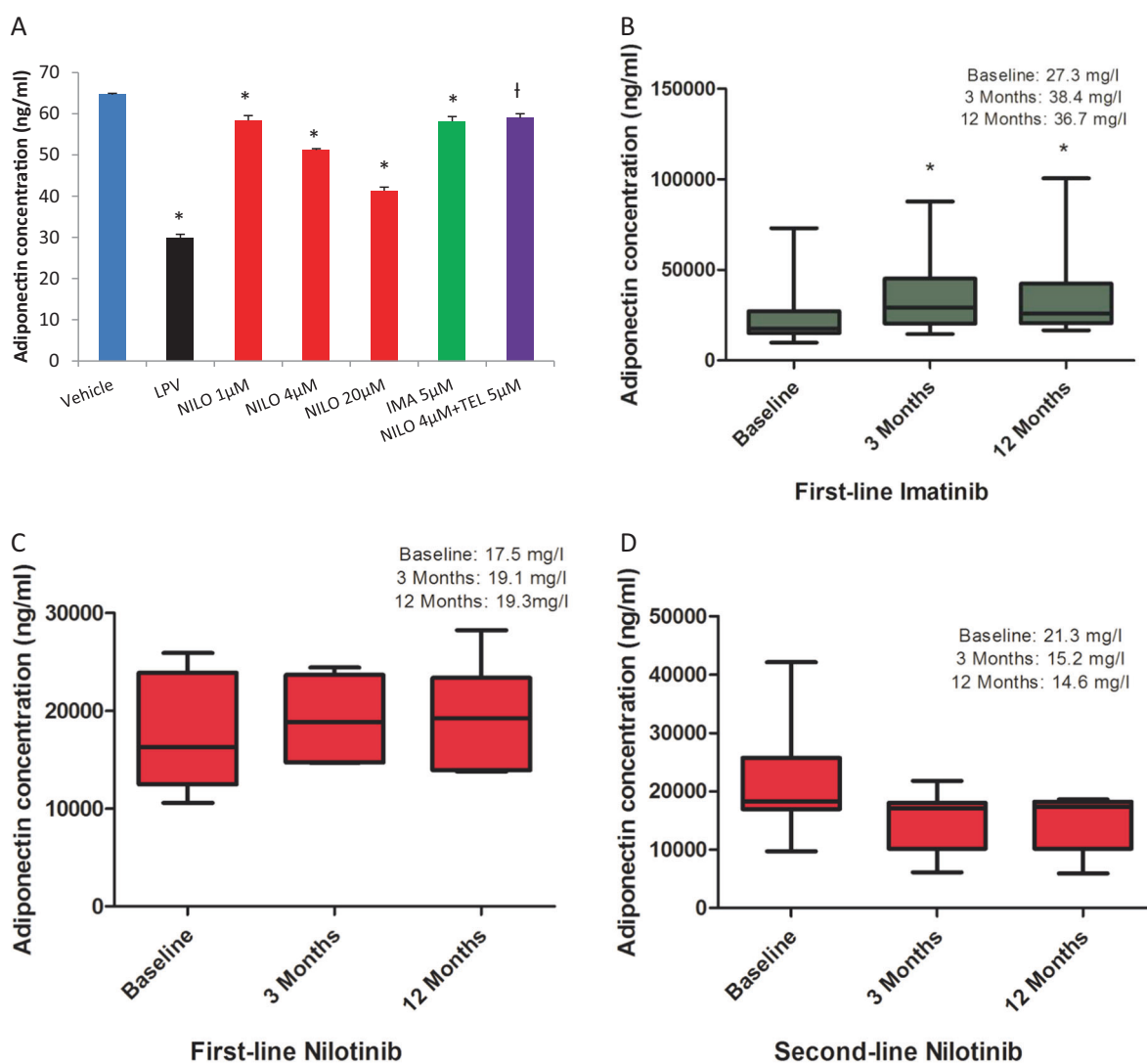


Fig. 2 Effect of nilotinib and imatinib on adiponectin in vitro and in vivo. Effect of nilotinib (with and without telmisartan) and imatinib on secreted adiponectin in differentiating 3T3-F442A adipocytes (A); plasma adiponectin levels at baseline, 3 months and 12 months in CML patients treated with imatinib (B); first-line nilotinib (C) and second-line nilotinib (D). Telmisartan was co-incubated with only one concentration of nilotinib (4 μ M). Lopinavir (LPV), an anti-HIV drug, was used as a positive control in vitro. All in vitro experiments were

repeated three times in triplicate. One-way ANOVA with Dunnett's Test was used for in vitro statistical analysis; Repeated measures ANOVA with Dunnett's Test was used to compare plasma adiponectin levels at different time points in CML patients. Data represent Mean \pm SD; $p \leq 0.05$. *Vehicle vs NILO/LPV/IMA; [†]NILO4 μ M vs NILO4 μ M + TEL5 μ M (in vitro). Mean adiponectin levels in each patient group at different time points were compared against the baseline value. NILO: nilotinib, IMA: imatinib, TEL: telmisartan, LPV: lopinavir

encodes a magnesium-ion-dependent phosphatidic acid phosphohydrolase enzyme, is involved in triglyceride synthesis [12]; *SREBP1* plays a role in cholesterol homeostasis [13]. We then assessed the effect of these two TKIs on *Glut4*, the principal glucose transporter in the adipocyte; both nilotinib ($p = 0.01$), and to a lesser extent imatinib ($p = 0.02$), significantly downregulated *Glut4* mRNA expression in differentiating adipocytes (Fig. 1B). Downregulation of *Glut4* by nilotinib could result in reduced glucose uptake into the adipocyte and may lead to insulin resistance observed in CML patients. Downregulation of *Glut4* by imatinib, a drug that has been consistently suggested to improve insulin sensitivity in

CML patients [14], is interesting; this suggests the need to assess other mechanisms involved in the regulation of whole body insulin sensitivity, such as the role of liver and skeletal muscle. We then assessed whether telmisartan can reverse nilotinib-induced adipocyte toxicity; co-incubation of telmisartan (5 μ M) with 4 μ M nilotinib resulted in significant reversal of nilotinib-mediated inhibition of adipocyte lipid accumulation (NILO + TEL: 0.52 ± 0.01 , in comparison to NILO 4 μ M: 0.46 ± 0.02 , $p = 0.01$; Fig. 1A) and adipogenic mRNA downregulation ($p = 0.02$; Fig. 1B).

Next, we investigated whether TKIs affect adiponectin in vitro and in plasma samples obtained from CML patients.

Adiponectin is a protein exclusively secreted by the adipocyte and is a key mediator of systemic insulin sensitivity and glucose homeostasis [6]. Total adiponectin in the conditioned media collected from drug-treated and control adipocytes were measured using a standard ELISA. Nilotinib induced a dose-dependent reduction in adiponectin secretion (4 μ M: 20% reduction, $p = 0.02$); however, the effect of imatinib was only marginal (9.9% reduction, $p = 0.04$). Interestingly, co-incubation of telmisartan with nilotinib reversed the inhibitory effect of nilotinib on adiponectin secretion in vitro ($p = 0.001$; Fig. 2A).

For the in vivo analysis of adiponectin, nonfasted plasma samples at three different time points (baseline, 3 and 12 months) were obtained from 30 CML patients who received either nilotinib ($n = 14$) or imatinib ($n = 16$) for at least 12 months. Relevant ethics approval and patient consent were obtained. All patients were in first chronic phase throughout. In the nilotinib-treated group, six patients received the drug as first-line therapy and eight as second line following initial treatment with imatinib. Five out of the eight second-line nilotinib patients were imatinib-resistant and showed higher *BCR-ABL1* transcript levels at the time of the switch; the remaining three were switched due to imatinib intolerance. In all second-line nilotinib patients, the sample collected at the time of initiation of nilotinib therapy was considered as the baseline sample. All patients in the imatinib-treated group received the drug as first-line. We did not have baseline sample for one of the imatinib-treated patients, therefore we excluded that patient from any analysis (i.e. imatinib, final $n = 15$). The median ages of imatinib and nilotinib-treated CML patients were 39 and 49 years, respectively; both drug groups had eight female subjects each. None of the patients recruited had a medical history of diabetes. Total adiponectin was measured using an electrochemiluminescence-based sandwich immunoassay (Meso Scale Discovery, USA). Repeated measures ANOVA with Dunnett's Test was used to compare adiponectin levels at different time points. Imatinib resulted in a significant increase in plasma adiponectin levels at 3 (38.4 ± 7.1 mg/l; $p < 0.01$) and 12 month (36.7 ± 7.2 mg/l; $p < 0.01$) time points compared with baseline values (27.3 ± 5.7 mg/l; $p < 0.05$; Fig. 2B). By contrast, in both first-line (Fig. 2C) and second-line (Fig. 2D) nilotinib patients, there was no change in adiponectin concentrations; however, with second-line nilotinib, there was a non-significant decrease at both 3 (15.2 ± 1.8 mg/l; $p = \text{NS}$) and 12 months (14.6 ± 1.7 mg/l; $p = \text{NS}$; Fig. 2D) when compared to baseline levels (21.3 mg/l).

Nilotinib-induced reduction in adiponectin in vitro was, to a certain extent, mirrored in the CML plasma samples obtained from second-line nilotinib-treated CML patients, but this was non-significant. However, it should be noted that our sample size was small ($n = 14$ or 15 per drug group) and therefore lacked sufficient power to detect a statistically significant

difference in adiponectin. On the other hand, the increase in plasma adiponectin observed with imatinib correlates with what has been previously reported for imatinib in CML patients [14]. Adiponectin expression is directly regulated by *PPAR γ* [6]; it is possible that nilotinib-induced reduction in adiponectin could be a direct result of the downregulation of *PPAR γ* by nilotinib. The molecular mechanism(s) by which imatinib increases adiponectin secretion is not clear; it is also possible that the increase in adiponectin levels observed with imatinib in vivo could be a mere reflection of improvement in general health in CML patients.

Here we have shown that repeated exposure of nilotinib and imatinib has contrasting effects on adipocyte lipid accumulation, adipogenic mRNA expression and secretion of adiponectin. Together, these mechanisms may explain the impaired glucose and lipid metabolism observed in nilotinib-treated CML patients. Although aggressive screening for cardiovascular risk factors and cardiometabolic surveillance in CML patients has been suggested to reduce nilotinib-related cardiometabolic events [15], there is also a need for therapeutic preventive strategies. The reversal of nilotinib-induced adipocyte toxicity by telmisartan in vitro is important in this context. The metabolic beneficial effects of telmisartan have been suggested to be due to both *PPAR γ* agonism [8] and angiotensin receptor blockade; the potential therapeutic utility of telmisartan to counter the deleterious cardiometabolic adverse effects caused by nilotinib in CML patients will now need to be evaluated by observational, as well as randomised studies. Our in vivo study has some major limitations, such as small sample size, non-availability of fasting plasma samples and lack of complete concurrent clinical data; future studies will need to address these limitations and validate these results to obtain a better understanding of nilotinib-induced metabolic adverse effects.

Acknowledgements This work was funded by Wellcome Trust Institutional Strategic Support Fund.

Author contributions SP, REC and MP conceptualised and designed the study. SS, EO, TF and SP conducted the experimental work and analysis. REC, KK and LW carried out the recruitment of patients and collection of samples and the clinical data. SP, REC, MP, SS and EO interpreted the data. SS, EO, LW, TF, KK, MP, REC and SP drafted the article. All authors had access to the final draft manuscript and approved the submission of the article.

Compliance with ethical standards

Conflict of interest The authors declare that they have no conflict of interest.

Open Access This article is licensed under a Creative Commons Attribution 4.0 International License, which permits use, sharing, adaptation, distribution and reproduction in any medium or format, as long as you give appropriate credit to the original author(s) and the source, provide a link to the Creative Commons license, and indicate if

changes were made. The images or other third party material in this article are included in the article's Creative Commons license, unless indicated otherwise in a credit line to the material. If material is not included in the article's Creative Commons license and your intended use is not permitted by statutory regulation or exceeds the permitted use, you will need to obtain permission directly from the copyright holder. To view a copy of this license, visit <http://creativecommons.org/licenses/by/4.0/>.

References


1. Saglio G, Kim DW, Issaragrisil S, le Coutre P, Etienne G, Lobo C, et al. Nilotinib versus imatinib for newly diagnosed chronic myeloid leukemia. *N Engl J Med*. 2010;362:2251–9.
2. Breccia M, Muscaritoli M, Gentilini F, Latagliata R, Carosino I, Rossi Fanelli F, et al. Impaired fasting glucose level as metabolic side effect of nilotinib in non-diabetic chronic myeloid leukemia patients resistant to imatinib. *Leuk Res*. 2007;31:1770–2.
3. Hochhaus A, Saglio G, Hughes TP, Larson RA, Kim DW, Issaragrisil S, et al. Long-term benefits and risks of frontline nilotinib vs imatinib for chronic myeloid leukemia in chronic phase: 5-year update of the randomized ENESTnd trial. *Leukemia*. 2016;30:1044–54.
4. Racil Z, Razga F, Drapalova J, Buresova L, Zackova D, Palackova M, et al. Mechanism of impaired glucose metabolism during nilotinib therapy in patients with chronic myelogenous leukemia. *Haematologica*. 2013;98:e124–26.
5. Aichberger KJ, Herndlhofer S, Scherthaner GH, Schillinger M, Mitterbauer-Hohendanner G, Sillaber C, et al. Progressive peripheral arterial occlusive disease and other vascular events during nilotinib therapy in CML. *Am J Hematol*. 2011;86:533–9.
6. Rosen ED, Spiegelman BM. Adipocytes as regulators of energy balance and glucose homeostasis. *Nature*. 2006;444:847–53.
7. Ravussin E, Smith SR. Increased fat intake, impaired fat oxidation, and failure of fat cell proliferation result in ectopic fat storage, insulin resistance, and type 2 diabetes mellitus. *Ann N Y Acad Sci*. 2002;967:363–78.
8. Pushpakom SP, Adaikalakoteswari A, Owen A, Back DJ, Tripathi G, Kumar S, et al. Telmisartan reverses antiretroviral-induced adipocyte toxicity and insulin resistance in vitro. *Diab Vasc Dis Res*. 2018;15:233–42.
9. Takagi H, Niwa M, Mizuno Y, Goto SN, Umamoto T. Telmisartan as a metabolic sartan: the first meta-analysis of randomized controlled trials in metabolic syndrome. *J Am Soc Hypertens*. 2013;7:229–35.
10. Virtue S, Vidal-Puig A. Adipose tissue expandability, lipotoxicity and the Metabolic Syndrome—an allostatic perspective. *Biochim Biophys Acta*. 2010;1801:338–49.
11. Rosen ED, MacDougald OA. Adipocyte differentiation from the inside out. *Nat Rev Mol Cell Biol*. 2006;7:885–96.
12. Fang Z, Wang S, Du X, Shi P, Huang Z. Phosphatidate phosphatase-1 is functionally conserved in lipid synthesis and storage from human to yeast. *Acta Biol Hung*. 2014;65:481–92.
13. Kim JB, Spiegelman BM. ADD1/SREBP1 promotes adipocyte differentiation and gene expression linked to fatty acid metabolism. *Genes Dev*. 1996;10:1096–107.
14. Fitter S, Vandyke K, Schultz CG, White D, Hughes TP, Zannettino AC. Plasma adiponectin levels are markedly elevated in imatinib-treated chronic myeloid leukemia (CML) patients: a mechanism for improved insulin sensitivity in type 2 diabetic CML patients? *J Clin Endocrinol Metab*. 2010;95:3763–7.
15. Aghel N, Delgado DH, Lipton JH. Cardiovascular toxicities of BCR-ABL tyrosine kinase inhibitors in chronic myeloid leukemia: preventive strategies and cardiovascular surveillance. *Vasc Health Risk Manag*. 2017;13:293–303.

Leukemia (2019) 33:1814–1816

<https://doi.org/10.1038/s41375-019-0393-0>

Acute myeloid leukemia

Peripheral blood minimal/measurable residual disease assessed in flow cytometry in acute myeloblastic leukemia

Cécile Guénot^{1,2} · Francis Lacombe³ · Kaoutar Allou³ · Florent Dumezy⁴ · Jean Feuillard⁵ · Franck Geneviève⁶ · Estelle Guérin⁵ · Julien Guy⁷ · Marc Maynadié⁷ · Oriane Wagner Ballon⁸ · Claude Preudhomme⁴ · André Baruchel⁹ · Hervé Dombret¹⁰ · Norbert Ifrah¹¹ · Marie C. Béné¹  · on behalf of the Groupe d'Etude Immunologique des Leucémies (GEIL)

Received: 14 July 2018 / Revised: 15 December 2018 / Accepted: 7 January 2019 / Published online: 5 February 2019

© Springer Nature Limited 2019

✉ Marie C. Béné
mariebene@gmail.com
mariechristine.bene@chu-nantes.fr

¹ Hematology Biology, University Hospital, Nantes, France

² Biology Laboratory, General Hospital, Le Mans, France

³ Hematology Biology, University Hospital, Bordeaux, France

⁴ Hematology Biology, University Hospital, Lille, France

⁵ Hematology Biology, University Hospital, Limoges, France

⁶ Hematology Biology, University Hospital, Angers, France

⁷ Hematology Biology, University Hospital, Dijon, France

⁸ Hematology Biology, University Hospital, Creteil, France

⁹ Hematology Department, Hôpital Robert Debré, Paris, France

¹⁰ Hematology Department, Hôpital Saint Louis, Paris, France

¹¹ Hematology Department, University Hospital, Angers, France

To the Editor:

There are unsolved questions in the field of minimal/measurable residual disease (MRD) detection by multi-parameter flow cytometry (MFC) in acute myeloblastic leukemia (AML). One of them, the value of peripheral blood (PB) testing, is raised repeatedly [1]. A Pubmed search on the topic is, however, exceedingly frustrating and mostly retrieves publications based on the morphological assessment of blast cells in PB [2–4]. The 2007 study by Maurillo et al. [5] was the first to propose pertinent MFC data. In this work, 50 and 48 patients, respectively, were studied in MFC for matched samples of PB and bone marrow (BM) after induction and consolidation of a chemotherapy regimen. At that time, all post-induction PB and BM samples contained detectable MRD. However, the 10 patients who had no detectable PB MRD after consolidation had a significantly better outcome, highlighting the potential value of PB MRD. In 2009, very early detection of peripheral blasts in MFC during the first days of induction was also shown to be of high prognostic value [6], a result confirmed by Yu et al. in 2015 [7]. The second most pertinent work of MRD during and after chemotherapy appeared in *Leukemia* in 2016, from the Dutch group HOVON [8]. The relevance of MRD assessment in PB on survival was confirmed there on a larger series of 76 evaluable patients. Among them, at a threshold of 0.04% established by ROC curves, respectively, 9/55 and 2/29 patients had detectable PB MRD after induction and consolidation. Their outcome was significantly poorer than that of MRD-negative patients. A good correlation was also noted with BM MRD.

In the course of a multicenter research program on AML MRD that was supported by the French Institute of Cancer (Inca), peripheral blood (PB) sampling was recommended for an ancillary investigation, besides that of classical bone marrow (BM) assessment. Results of the latter have been published recently [9], detailing the types of patients and treatments received. This work demonstrated the robustness of a novel analysis algorithm using a patient-tailored protocol established with MFC data of the diagnosis and a fixed set of monoclonal antibodies. Being then directly applied to the same patient's follow-up samples, this protocol allowed to detect MRD down to a level of 5×10^{-5} . Patients who never had an MRD above this threshold during follow-up fared significantly better than those having at least one "positive" follow-up sample.

Here we report the application of the same strategy for the 96 patients of this cohort who also benefited from PB sampling and who are representative of the whole 256 cohort. PB samples were treated and analyzed exactly as the BM samples, as reported [9], in a lysis-no-wash approach and the recommendation to acquire at least 250,000 events.

Failure to detect more than 10 suspect immunophenotypically clustered events (usually none at all) led to the conclusion of "undetectable" MRD. All analyses were performed blinded of the results of BM MRD data. The diagnosis listmodes of each patient were completely reinterpreted to establish the appropriate patient-specific protocol. Overall, 217 follow-up samples were analyzed, respectively, 66 post-induction, 55 before the second consolidation, 35 at the end of treatment, and 61 at later time-points. MRD was found to be always negative for 67 patients, while it was always positive for 25. For the remaining four patients, MRD became negative for three and all ultimately relapsed. These patients were pooled with the group of MRD-positive patients, compared to the truly "always negative" mentioned above.

Event-free survival was assessed from the date of complete remission until relapse, death, or last news. Overall survival was assessed from the date of complete remission until death or last news. The Medcalc® (Ostend, Belgium) software was used to perform log rank tests and Kaplan Meier graphical representations. This confirmed the significantly better outcome associated to constantly negative PB MRD (median overall survival not reached vs. 26 months for positive patients [95% CI 16–41], $p = 0.0002$; Fig. 1a). The same good prognostic value was observed even when considering only the 66 patients tested at the end of induction (MRD1; median overall survival not reached vs. 20 months for positive patients [95% CI 16–41], $p = 0.0009$; Fig. 1b). The dates of sample collection were too heterogeneous to test other time-points in this "real life" collection of data (i.e., independent of any clinical trial), yet the same prognostic value was observed. We also tested other thresholds which, as for the BM study of the same cohort, demonstrated the clear superiority of "undetectable" MRD at the 5×10^{-5} sensitivity.

Agreement between PB and BM results was investigated for 213 matched samples available. For 144 pairs of them, both PB and BM were always negative, and for 54 both pairs were always positive. The remaining 15 samples has no detectable PB MRD while it was positive in BM. This resulted in a specificity and positive predictive value of 100%, while sensitivity was 78% and the negative predictive value 91%.

In conclusion, this multicenter study confirms the robustness and universal applicability of the limited panel used, where the relevant myeloid markers are CD34, CD117, CD33 and CD13, CD15, and CD7 being less informative [9]. Of course, an initial CD45 gating is crucial to properly identify the progenitor population. This is consistent with the recently published consensus of the European LeukemiaNet [1]. As suggested by the studies analyzing the rate of blast decrease in PB during the first days of induction chemotherapy [2–4, 6, 7], this work

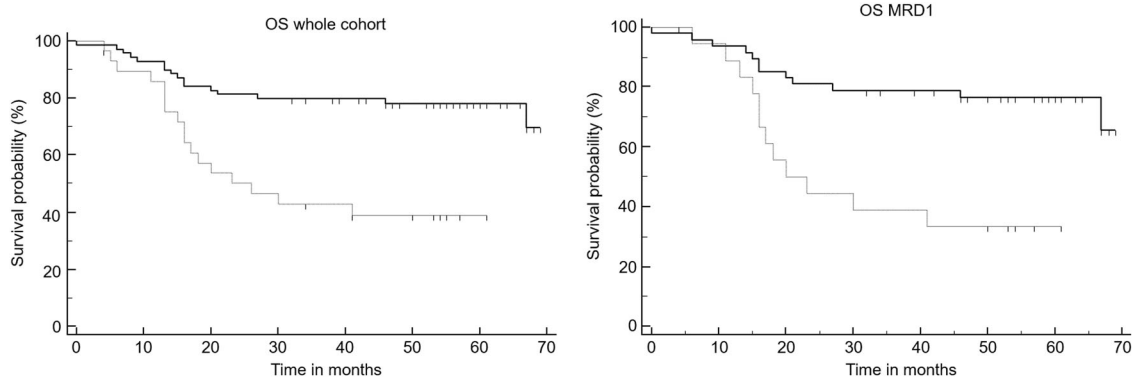


Fig. 1 Overall survival in patients with persistent undetectable MRD (full lines) and patients with detectable MRD at least in one sample (dotted line) for the whole cohort (left) and for patients with

undetectable MRD (full lines) or detectable MRD (dotted line) at MRD1. $p = 0.0002$ and 0.0009 , respectively

confirms the importance of a rapid clearance of the tumor bulk. Indeed, the best prognosis is definitely obtained for patients with undetectable MRD as early as at the first point of investigation, who then retain negative MRD. PB is more easily available than BM and simpler to analyze because there are no normal progenitors in such samples. It could thus be suggested to perform MRD detection in PB in order to reinforce therapy in case of positivity. BM MRD could thus become necessary only in case of PB negativity, to secure the good response of individual patients.

Compliance with ethical standards

Conflict of interest The authors declare that they have no conflict of interest.

Publisher's note: Springer Nature remains neutral with regard to jurisdictional claims in published maps and institutional affiliations.

References

1. Schuurhuis GJ, Heuser M, Freeman S, Béné MC, Buccisano L, Cloos J, et al. Minimal/measurable residual disease in AML: a consensus document from the European LeukemiaNet MRD working party. *Blood*. 2018;131:1275–1291.8.
2. Arellano M, Pakkala S, Langston A, Tighiouart M, Pan L, Chen Z, et al. Early clearance of peripheral blood blasts predicts response to induction chemotherapy in acute myeloid leukemia. *Cancer*. 2012; 118:5278–82.
3. Bertoli S, Bories P, Béné MC, Daliphard S, Lioure B, Pigneux A, Groupe Ouest-Est d'Etude des Leucémies Aiguës et Autres Maladies du Sang (GOELAMS), et al. Prognostic impact of day 15 blast clearance in risk-adapted remission induction chemotherapy for younger patients with acute myeloid leukemia: long-term results of the multicenter prospective LAM-2001 trial by the GOELAMS study group. *Haematologica*. 2014;99:46–53.
4. Short NJ, Benton CB, Chen HC, Qiu P, Gu L, Pierce S, et al. Peripheral blood blast clearance is an independent prognostic factor for survival and response to acute myeloid leukemia induction chemotherapy. *Am J Hematol*. 2016;91:1221–6.
5. Maurillo L, Buccisano F, Spagnoli A, Del Poeta G, Panetta P, Neri B, et al. Monitoring of minimal residual disease in adult acute myeloid leukemia using peripheral blood as an alternative source to bone marrow. *Haematologica*. 2007;92:605–11.
6. Lacombe F, Arnoulet C, Maynadié M, Lippert E, Luquet I, Pigneux A, et al. Early clearance of peripheral blasts measured by flow cytometry during the first week of AML induction therapy as a new independent prognostic factor: a GOELAMS study. *Leukemia*. 2009;23:350–7.
7. Yu C, Kong QL, Zhang YX, Weng XQ, Wu J, Sheng Y, et al. Clinical significance of day 5 peripheral blast clearance rate in the evaluation of early treatment response and prognosis of patients with acute myeloid leukemia. *J Hematol Oncol*. 2015;8:48.
8. Zeijlemaker W, Kelder A, Oussirren-Brockhopp YJM, Scholten WJ, Snel AN, Veldhuizen D, et al. Peripheral blood minimal residual disease may replace bone marrow minimal residual disease as an immunophenotypic biomarker for impending relapse in acute myeloid leukemia. *Leukemia*. 2016;30:708–15.
9. Lacombe F, Campos L, Allou K, Arnoulet C, Delabarthe A, Dumezy F, et al. Prognostic value of multicenter flow cytometry harmonized assessment of minimal residual disease in acute myeloblastic leukemia. *Hematol Oncol*. 2018;36:422–8.

Leukemia (2019) 33:1817–1821
<https://doi.org/10.1038/s41375-019-0396-x>

Multiple myeloma gammopathies

Genome-wide association study of monoclonal gammopathy of unknown significance (MGUS): comparison with multiple myeloma

Hauke Thomsen¹ · Subhayan Chattopadhyay¹ · Niels Weinhold^{2,3} · Pavel Vodicka^{4,5,6} · Ludmila Vodickova^{4,5,6} · Per Hoffmann^{7,8} · Markus M. Nöthen^{7,9} · Karl-Heinz Jöckel¹⁰ · Christian Langer¹¹ · Roman Hajek¹² · Göran Hallmans¹³ · Ulrika Pettersson-Kymmer¹⁴ · Claes Ohlsson¹⁵ · Florentin Späth¹⁶ · Richard Houlston^{17,18} · Hartmut Goldschmidt^{2,19} · Kari Hemminki¹ · Asta Försti¹

Received: 10 December 2018 / Revised: 10 January 2019 / Accepted: 21 January 2019 / Published online: 8 February 2019
© Springer Nature Limited 2019

To the Editor:

Monoclonal gammopathy of undetermined significance (MGUS) is a condition in which immunoglobulin-derived serum M-protein is produced by a plasma cell clone and is detectable in the blood [1]. MGUS resembles multiple myeloma (MM), but antibody levels and number of plasma cells in the bone marrow are lower, and it is generally asymptomatic and often diagnosed idiosyncratically. However, since MGUS can lead to MM, which develops at the rate of 0.5–1.5% a year, yearly monitoring is generally recommended [2]. The prevalence of MGUS increases from age 50 onwards (1.7% at 50–59 years), reaching 6.6% by age over 80 years according to a literature review [2]. As the cumulative incidence of MM by age 75 years in Sweden is 0.4% for men and 0.3% for women, it is clear that the prevalence of MGUS far exceeds that of MM (NORDCAN database <http://www-dep.iarc.fr/NORDCAN/FI/frame.asp>).

Genome-wide association studies (GWASs) have so far identified common genetic variants at 23 loci associated with MM risk [3]. Thus far the role of genetic variation influencing MGUS has only been studied to a limited extent [4]. Some of the first reported MM risk loci have in two early studies been shown to be at least weakly associated with MGUS [5]. To more comprehensively address the

genetics of MGUS and its relationship to MM we conducted a GWAS of MGUS by analyzing 992 patients and 2900 controls.

Detailed methods are described in the Supplement. We studied three independent sets of MGUS patients and controls. The German GWAS comprised 243 MGUS cases and 1285 controls [4]. The Czech GWAS was based on 288 cases and 600 controls. The Swedish MGUS included 461 patients and 1025 controls. Odds ratios (ORs) for single-nucleotide polymorphism (SNP) associations in the three populations were meta-analyzed using PLINK software v1.90. Differences in the associations between MGUS and MM were tested using ASSET as previously [5]. The most promising MGUS associations were tested in the meta-analysis of the German population of 1717 MM cases and 2069 controls and the UK population of 2282 MM cases and 5197 controls; a recent study describing 23 genome-wide significant loci for MM [3, 6].

A Manhattan plot of GWAS on MGUS highlights 10 loci reaching a meta p -value below 10^{-5} (Supplementary Figure 1). The meta ORs for the risk allele ranged from 1.28 to 1.48 and the smallest p -value reached 5.6×10^{-7} for locus 3p22.1 (rs9848754, *ULK4*) (Table 1). With the exception of this locus and the locus at 17p11.2 (rs74998556, *TNFRSF13B*), the other eight loci were unique to MGUS when compared to MM (95% confidence intervals (CIs) were non-overlapping). A similar conclusion was reached by the ASSET analysis, displaying MGUS on eight SNPs as positive and MM data as null or negative (Supplementary Figure 2). None of the signals from the three MGUS sample sets showed significant heterogeneity (p_{het} and I^2 statistic, Supplementary Table 1). Neither was heterogeneity observed for meta ORs for MM.

We compared GWAS associations for MGUS at the 23 loci for which genome-wide significant associations have

These authors contributed equally: K Hemminki, A Försti.

Supplementary information The online version of this article (<https://doi.org/10.1038/s41375-019-0396-x>) contains supplementary material, which is available to authorized users.

✉ Asta Försti
a.foersti@dkfz.de

Extended author information available on the last page of the article

been reported for MM (Table 2) [3]. ORs for 10 MGUS SNPs were nominally significant ($p < 0.05$) and the risk allele was the same as for MM. For 9 of these loci the OR for MGUS (considering also the best SNP for MGUS in high linkage disequilibrium with the MM SNP) was equal or higher than it was for MM and these included loci (marked by genes [3]): 2p23.3 (*DTNB*), 2q31.1 (*SP3*), 3p22.1 (*ULK4*), 6p22.3 (*JARID2*), 7q36.1 (*ABCF2*), 8q24.21 (*MYC*), 9p21.3 (*MTAP*), 17p11.2 (*TNFRSF13B*), and 19p13.11 (*KLF2*). The 95% CIs of MGUS ORs included the OR of MM at each of these loci. For 10 other SNPs the ORs were at least marginally higher for MM than for MGUS and the risk alleles were identical but the upper 95% CI of the MGUS SNPs covered the OR for MM. For 4 SNPs (16q23.1, 20q13.13, 22q13, and 22q13.1 marked by gene *CBX7*) the ORs for MM were substantially higher than those for MGUS for which the ORs were close to unity (1.00).

The data from Table 2 were subjected to ASSET analysis, and as expected all MM associations were classified as positive (Supplementary Figure 3). Among MGUS SNPs, 16 were also classified as positive, 4 as null (rs6595443, rs17507636, rs13338946, and rs877529), and 3 as negative (rs7193541, rs6066835, and rs138740) (Table 2, column “MGUS OR”). Only for rs6066835 and rs138740 the 95% CIs did not overlap between MGUS and MM.

The results are summarized in Supplementary Figure 4 for each of the 31 loci. The 8 MGUS-specific loci are marked with stars. Functional considerations of the associated SNPs are based on data from the available annotation tools (Supplement).

In the interpretation of the genetic profiles between the two plasma cell dyscrasias one needs to consider the prevalence of these conditions, MGUS being more than 10 times more common than MM. Thus, a higher OR for a SNP in MGUS compared to MM may imply that the related gene predisposes to MGUS but does not contribute to progression to the end disease. If the OR for the SNP is increased to an equal extent in MGUS and MM, the SNP is likely to be predisposing equally to MGUS and to the end disease. If the risk is increased only in MM the related gene is likely to be predisposing to it. A large difference between the risk for MGUS and the end disease may indicate selection towards the risk genotype. A limitation of the study is that we have longitudinal follow-up data for a relatively short time not allowing flagging of the MGUS cases developing MM.

Applying these guidelines, and keeping in mind the caveat of limited sample sizes, the data suggest eight loci to be specific to MGUS. These included four loci, which marked genes *SGMS2*, *RIMS2*, and *TSNARE1*, and one with limited biological data. The four other loci marked genes that had known functions in cancer: *PROX1*, *SFMBT*,

Table 1 Meta-analyzed odds ratios for the most significant MGUS SNPs ($p < 10^{-5}$) compared with meta-analyzed odds ratios for MM

Chromosomal band	SNP	Base pair (hg.19)	Risk allele	MGUS			MM			GENCODE gene
				OR _{Meta}	95% CI	p-Value	OR _{Meta}	95% CI	p-Value	
1q32.3	rs3009934	214301323	T	1.32	1.18–1.48	2.0 × 10⁻⁰⁶	0.99	0.93–1.05	7.9 × 10⁻⁰¹	86 kb 3' of <i>PROX1</i>
3p22.1	rs9848754	41753647	T	1.44	1.25–1.67	5.6 × 10⁻⁰⁷	1.26	1.17–1.35	2.3 × 10⁻¹⁰	<i>ULK4</i> intron
3q13.11	rs73180532	104051156	C	1.28	1.15–1.42	6.8 × 10⁻⁰⁶	1.00	0.95–1.06	9.6 × 10⁻⁰¹	278 kb 5' of <i>AC016970.1</i>
4q25	rs72888948	108802381	T	1.48	1.25–1.76	5.1 × 10⁻⁰⁶	1.07	0.97–1.18	1.6 × 10⁻⁰¹	<i>SGMS2</i> intron
8q22.3	rs9656789	105068489	A	1.37	1.19–1.56	3.4 × 10⁻⁰⁶	1.04	0.97–1.12	2.6 × 10⁻⁰¹	<i>RIMS2</i> intron
8q24.3	rs4928692	143466597	G	1.38	1.21–1.59	2.5 × 10⁻⁰⁶	1.10	1.02–1.18	1.2 × 10⁻⁰²	<i>TSNARE1</i> intron
10p14	rs7920332	7250346	C	1.27	1.14–1.42	7.1 × 10⁻⁰⁶	1.00	0.93–1.08	9.1 × 10⁻⁰¹	<i>SFMBT2</i> intron
14q24.1	rs12436964	69108086	T	1.31	1.17–1.47	2.4 × 10⁻⁰⁶	1.06	1.00–1.13	4.0 × 10⁻⁰²	<i>RAD51B</i>
15q22.31	rs4561409	64535700	C	1.30	1.16–1.45	6.3 × 10⁻⁰⁶	0.97	0.92–1.03	4.0 × 10⁻⁰¹	<i>CSNK1G1</i> intron
17p11.2	rs74998556	16839782	T	1.46	1.25–1.69	9.0 × 10⁻⁰⁷	1.18	1.09–1.28	5.7 × 10⁻⁰⁵	<i>TNFRSF13B</i>

\hat{p}^2 values were consistent with homogeneity of all meta-analyzed ORs

P_{het} was >0.5 for all GWAS ORs

Bold values indicate significance at suggestive threshold of 10^{-5}

MGUS monoclonal gammopathy of unknown significance, MM multiple myeloma, *Igk19* human genome NCBI build 19, OR_{Meta} meta-analyzed odds ratio, CI confidence interval

Table 2 Published multiple myeloma risk loci in MGUS meta-analysis

Published SNP	Best MGUS SNP ^a	CHR	Associated gene ^b	Base-pair position (hg19)	Published MM OR ^c	MGUS OR ^d	95% CI	Meta <i>p</i>	Risk allele	Other allele	<i>D'</i>	<i>r</i> ²	<i>P</i> _{het} ^e	<i>I</i> ² ^e
rs6746082		2p23.3	DTNB	25659244	1.23 ^f	1.19	1.04–1.35	8.2 × 10⁻⁰³	A	C			0.46	0.00
rs4325816	rs201567111	2q31.1	SP3	25745570	1.12	1.31	1.15–1.49	3.3 × 10⁻⁰⁵	CT	C	0.71	0.36	0.63	0.00
rs1052501		3p22.1	ULK4	41925398	1.26 ^f	1.38	1.05–1.35	6.0 × 10⁻⁰³	T	C			0.79	0.00
rs10936599	rs9848754	3q26.2	ACTRT3, MYNN, LRR34	41753647	1.20 ^f	1.44	1.19–1.59	1.1 × 10⁻⁰⁵	C	T	1.00	1.00	0.30	18.07
rs56219066		5q15	ELL2	95242931	1.16 ^f	1.10	1.25–1.67	5.6 × 10⁻⁰⁷	T	C			0.32	12.07
rs6595443		5q23.2	CEP120	169492101	1.11	1.10	0.98–1.25	9.6 × 10 ⁻⁰²	C	T			0.69	0.00
rs34229995		6p22.3	JARID2	122743325	1.36	1.03	0.97–1.25	1.1 × 10 ⁻⁰¹	T	C			0.32	13.19
rs2285803		6p21.3	PSORS1C1, CCHCR1	15244018	1.21 ^f	1.37	0.92–1.14	6.4 × 10 ⁻⁰¹	A	T			0.24	29.18
rs9372120		6q21	ATG5, PRDMI	31107258	1.19	1.11	1.03–1.81	2.9 × 10⁻⁰²	G	C			0.39	0.00
rs4487645		7p15.3	DNAH11, CDCA7L	106667535	1.24	1.17	0.99–1.24	5.4 × 10 ⁻⁰²	T	C			0.47	0.00
rs17507636	rs56249828	7q22.3	CCDC71L	21944607	1.12	1.19	0.97–1.25	1.2 × 10 ⁻⁰¹	G	T			0.64	0.00
rs58618031		7q31.33	POT1	21938240	1.22	1.17	1.04–1.31	6.1 × 10⁻⁰³	C	A			0.59	0.00
rs7781265		7q36.1	ABCF2 , CHPF2 , SMARCD3	106291118	1.12	1.02	1.06–1.34	1.8 × 10⁻⁰³	T	C	0.95	0.87	0.85	0.00
rs1948915	rs219228	8q24.21	MYC	124583896	1.15	1.07	0.90–1.15	7.4 × 10 ⁻⁰¹	C	T			0.73	0.00
rs2811710		9p21.3	CDKN2A, MTAP , CDKN2B-AS1	150950940	1.14	1.15	0.95–1.20	2.4 × 10 ⁻⁰¹	T	C			0.08	60.92
rs2790457		10p12.1	WAC	150939396	1.11	1.25	1.03–1.43	1.9 × 10⁻⁰²	A	G			0.09	59.05
rs13338946		16p11.2	PRR14, FBR3 , SRCAP	128222421	1.15	1.20	1.08–1.43	1.7 × 10⁻⁰³	C	A	0.94	0.48	0.6	0.00
rs7193541		16q23.1	RFD3 , GLG1	21991923	1.12	1.15	1.07–1.33	1.5 × 10⁻⁰³	C	T			0.40	0.00
rs4273077		17p11.2	TNFRSF13B	28856819	1.30 ^f	1.40	1.02–1.28	1.6 × 10⁻⁰²	C	T			0.44	0.00
rs11086029	rs74998556	19p13.11	KLF2	30700858	1.14	1.10	0.97–1.24	1.1 × 10 ⁻⁰¹	G	A			0.40	0.00
rs6066835	rs71178685	20q13.13	PREX1	74664743	1.23	1.04	0.92–1.17	4.7 × 10 ⁻⁰¹	C	T			0.04	68.05
rs138740		22q13	HMGXB4, TOM1	16849139	1.21 ^f	0.98	0.87–1.09	7.2 × 10 ⁻⁰¹	T	C			0.57	0.00
rs877529		22q13.1	CBX7	16839782	1.22 ^f	1.40	1.19–1.64	2.8 × 10⁻⁰⁵	G	A			0.25	27.45
				16438661	1.14	1.46	1.25–1.69	9.0 × 10⁻⁰⁷	T	A	1.00	0.66	0.23	30.25
				16443718	1.14	1.17	1.03–1.33	1.5 × 10⁻⁰²	T	A			0.63	0.00
				47355009	1.23	1.21	1.06–1.39	4.3 × 10⁻⁰³	TA	T	0.97	0.90	0.76	0.00
				35699582	1.21 ^f	0.92	0.74–1.12	4.2 × 10 ⁻⁰¹	C	T			0.46	0.00
				39542292	1.22 ^f	0.96	0.85–1.06	4.1 × 10 ⁻⁰¹	C	T			0.51	0.00
					1.22 ^f	1.08	0.96–1.19	1.7 × 10 ⁻⁰¹	A	G			0.78	0.00

MGUS monoclonal gammopathy of unknown significance, MM multiple myeloma, SNP single-nucleotide polymorphism, *IgH19* human genome NCBI build 19, *OR*_{Meta} meta-analyzed odds ratio, *CI* confidence interval

^aIn case published SNP did not give the strongest signal

^bCandidate causal gene, suggested by Went et al. [3], is indicated in bold

^cWent et al. [3]

^dO = null in ASSET analysis; N = negative in ASSET analysis

^e*P*_{het} and *I*² values were calculated for heterogeneity between the MGUS populations

^fIn Went et al. the best SNP in the risk locus differs from the previously published one

Meta *p* values < 0.05 are indicated in bold

RAD51B, and *CSNK1G1*. *PROX1* interacts with *GATA2*, an important regulator of hematopoiesis and roles in predisposition to myelodysplastic syndrome/acute myeloid leukemia [7]. *SFMBT* is a polycomb group epigenetic regulator with suggested functions in prostate cancer. The DNA repair gene *RAD51C* has been associated with germline mutations in common cancers [8, 9]. Casein kinase 1 gamma 1 isoforms contribute plasma cell survival [10–12]. According to the above convention these genes may be important in MGUS but the variants are selected against during progression to the end diseases.

The second group of SNPs was shared by the two dyscrasias and ORs tended to be higher in MGUS than in MM. These included SNPs marking *DTNB*, a gene encoding a component of the dystrophin-associated protein complex, *ULK4*, encoding a key regulator of mTOR-mediated autophagy [13], and *TNFRSF13B* encoding a key regulator of B- and T-cell functions with involvement in pathophysiology of MM [14]. The association of rs4487645 (IRF4-binding site) was weaker for MGUS than for MM while for rs11086029 (19p13.11, *KLF2*) the association was slightly higher. The data suggest that the underlying gene functions are vital for MGUS and MM but they appear most important for the end disease.

As the final group, the SNPs marked by genes, *PREX1* and *TOM1*, were not MGUS related. However, it is intriguing that *PREX1* appeared as a major interacting partner when genome-wide two gene interactions were tested in MGUS [15]; in the same study *TOM1L1*, an analog of *TOM1* was also a significant interaction partner. Individually, neither *PREX1* nor *TOM1* associated with MGUS in this or in the earlier study [4]. If the role of *PREX1* or *TOM1* could be replicated in a larger interaction study the combined results could be explained with a model of higher enrichments of functional variants in the end disease. Additionally, SNPs marked by genes *CEP120*, *CBX7*, and *RFWD3* were enriched in MM compared to MGUS.

In summary, the present GWAS on MGUS appears to be capable of delineating distinctions between MGUS and MM germlines. Associations with the *PROX1*, *SFMBT*, *RAD51B*, and *CSNK1G1* loci were only found for MGUS, which may suggest that they are less important in the course of progression to MM. These genes have known functions in plasma cells and/or carcinogenesis, including homeobox transcription factor (*PROX1*) interacting with *GATA2*, chromatin remodeling through histone modification (*SFMBT*), double-stranded DNA repair (*RAD51B*), and cell cycle checkpoint arrest, DNA repair, and Wnt signaling (*CSNK1G1*). These are the functions that have been proposed to the SNPs identified in MM (chromatin remodeling, B-cell development, and cell cycle/genomic stability); additionally, apoptosis/autophagy pathways were suggested

for MM for which we did not find evidence in MGUS [3]. The association with *TNFRSF13* was stronger in MGUS compared to MM but the reverse was the case for the SNP forming the IRF4-binding site. *PREX1* and *TOM1* associations were only found in MM. If such distinctions can be verified in independent studies on MGUS they advance molecular understanding of the progression process, of the related prognostic markers and of the possible targets for intervention.

Acknowledgements Supported by Multiple Myeloma Research Foundation, the German Ministry of Education and Science (01ZX1309B), the Harald Huppert Foundation, and Deutsche Krebshilfe. Research by the Houlston Group is supported by grants from myeloma UK and BLOODWISE. PV and LV are recipients of a support from UNCE-MED006 and PROGRESS Q28.

Compliance with ethical standards

Conflict of interest The authors declare that they have no conflict of interest.

Publisher's note: Springer Nature remains neutral with regard to jurisdictional claims in published maps and institutional affiliations.

References

- Merlini G, Palladini G. Differential diagnosis of monoclonal gammopathy of undetermined significance. *Hematology Am Soc Hematol Educ Program*. 2012;2012:595–603.
- Wadhwa RK, Rajkumar SV. Prevalence of monoclonal gammopathy of undetermined significance: a systematic review. *Mayo Clin Proc*. 2010;85:933–42.
- Went M, Sud A, Forst A, Halvarsson BM, Weinhold N, Kimber S, et al. Identification of multiple risk loci and regulatory mechanisms influencing susceptibility to multiple myeloma. *Nat Commun*. 2018;9:3707.
- Thomsen H, Campo C, Weinhold N, Filho MI, Pour L, Gregora E, et al. Genome-wide association study on monoclonal gammopathy of unknown significance (MGUS). *Eur J Haematol*. 2017;99:70–9.
- Weinhold N, Johnson DC, Rawstron AC, Forst A, Doughty C, Vijayakrishnan J, et al. Inherited genetic susceptibility to monoclonal gammopathy of unknown significance. *Blood*. 2014;123:2513–7.
- Chubb D, Weinhold N, Broderick P, Chen B, Johnson DC, Forst A, et al. Common variation at 3q26.2, 6p21.33, 17p11.2 and 22q13.1 influences multiple myeloma risk. *Nat Genet*. 2013;45:1221–5.
- Kazenwadel J, Betterman KL, Chong CE, Stokes PH, Lee YK, Secker GA, et al. *GATA2* is required for lymphatic vessel valve development and maintenance. *J Clin Invest*. 2015;125:2979–94.
- Golmard L, Castera L, Krieger S, Moncoutier V, Abidallah K, Tenreiro H, et al. Contribution of germline deleterious variants in the *RAD51* paralogs to breast and ovarian cancers. *Eur J Hum Genet*. 2017;25:1345–53.
- Bennett JA, Braga AC, Pinto A, Van de Vijver K, Comejo K, Pesci A, et al. Uterine PEComas: a morphologic, immunohistochemical, and molecular analysis of 32 tumors. *Am J Surg Pathol*. 2018;42:1370–83.

10. Bjorklund CC, Ma W, Wang ZQ, Davis RE, Kuhn DJ, Kornblau SM, et al. Evidence of a role for activation of Wnt/beta-catenin signaling in the resistance of plasma cells to lenalidomide. *J Biol Chem.* 2011;286:11009–20.
11. Manni S, Carrino M, Manzoni M, Giansin K, Nunes SC, Costacurta M, et al. Inactivation of CK1alpha in multiple myeloma empowers drug cytotoxicity by affecting AKT and beta-catenin survival signaling pathways. *Oncotarget.* 2017;8:14604–19.
12. Hu Y, Song W, Cirstea D, Lu D, Munshi NC, Anderson KC. CSNK1alpha1 mediates malignant plasma cell survival. *Leukemia.* 2015;29:474–82.
13. Lebovitz CB, Robertson AG, Goya R, Jones SJ, Morin RD, Marra MA, et al. Cross-cancer profiling of molecular alterations within the human autophagy interaction network. *Autophagy.* 2015;11:1668–87.
14. Hengeveld PJ, Kersten MJ. B-cell activating factor in the pathophysiology of multiple myeloma: a target for therapy? *Blood Cancer J.* 2015;5:e282.
15. Chattopadhyay S, Thomsen H, da Silva Filho MI, Weinhold N, Hoffmann P, Nothen MM, et al. Enrichment of B cell receptor signaling and epidermal growth factor receptor pathways in monoclonal gammopathy of undetermined significance: a genome-wide genetic interaction study. *Mol Med.* 2018;24:30.

Affiliations

Hauke Thomsen¹ · Subhayan Chattopadhyay¹ · Niels Weinhold^{2,3} · Pavel Vodicka^{4,5,6} · Ludmila Vodickova^{4,5,6} · Per Hoffmann^{7,8} · Markus M. Nöthen^{7,9} · Karl-Heinz Jöckel¹⁰ · Christian Langer¹¹ · Roman Hajek¹² · Göran Hallmans¹³ · Ulrika Pettersson-Kymmer¹⁴ · Claes Ohlsson¹⁵ · Florentin Späth¹⁶ · Richard Houlston^{17,18} · Hartmut Goldschmidt^{2,19} · Kari Hemminki¹ · Asta Försti¹

¹ Division of Molecular Genetic Epidemiology, German Cancer Research Center (DKFZ), Im Neuenheimer Feld 580, D-69120 Heidelberg, Germany

² Department of Internal Medicine V, University of Heidelberg, Heidelberg, Germany

³ Myeloma Institute, University of Arkansas for Medical Sciences, Little Rock, AR, USA

⁴ Institute of Experimental Medicine, Academy of Sciences of the Czech Republic, Videnska 1083, 142 00 Prague, Czech Republic

⁵ Institute of Biology and Medical Genetics, 1st Medical Faculty, Charles University, Albertov 4, 128 00 Prague, Czech Republic

⁶ Faculty of Medicine and Biomedical Center in Pilsen, Charles University in Prague, 30605 Pilsen, Czech Republic

⁷ Institute of Human Genetics, University of Bonn, Bonn, Germany

⁸ Department of Biomedicine, University of Basel, Basel, Switzerland

⁹ Department of Genomics, Life & Brain Research Center, University of Bonn, Bonn, Germany

¹⁰ Institute for Medical Informatics, Biometry and Epidemiology, University Hospital Essen, University of Duisburg-Essen, Essen, Germany

¹¹ Department of Internal Medicine III, University of Ulm, Ulm, Germany

¹² Department of Hematooncology, University Hospital Ostrava, 17. listopadu 1790, 708 52 Ostrava, Czech Republic

¹³ Department of Medical Biosciences/Pathology, University of Umea, Umea, Sweden

¹⁴ Clinical Pharmacology, Department of Pharmacology and Clinical Neuroscience, Umea University, Umea, Sweden

¹⁵ Centre for Bone and Arthritis Research, Department of Internal Medicine and Clinical Nutrition, Institute of Medicine, Sahlgrenska Academy, University of Gothenburg, Gothenburg, Sweden

¹⁶ Department of Radiation Sciences, Oncology, Umeå University, Umeå, Sweden

¹⁷ Division of Genetics and Epidemiology, The Institute of Cancer Research, London, UK

¹⁸ Division of Molecular Pathology, The Institute of Cancer Research, London, UK

¹⁹ National Centre of Tumor Diseases, Heidelberg, Germany

Leukemia (2019) 33:1822–1827
<https://doi.org/10.1038/s41375-019-0398-8>

Acute myeloid leukemia

Destabilization of AETFC through C/EBP α -mediated repression of LYL1 contributes to t(8;21) leukemic cell differentiation

Meng-Meng Zhang¹ · Na Liu² · Yuan-Liang Zhang¹ · Bowen Rong³ · Xiao-Lin Wang¹ · Chun-Hui Xu² · Yin-Yin Xie¹ · Shuhong Shen⁴ · Jiang Zhu¹ · Stephen D. Nimer⁵ · Zhu Chen¹ · Sai-Juan Chen¹ · Robert G. Roeder⁶ · Fei Lan³ · Lan Wang² · Qiu-Hua Huang¹ · Xiao-Jian Sun¹

Received: 3 August 2018 / Revised: 25 November 2018 / Accepted: 21 January 2019 / Published online: 12 February 2019
 © Springer Nature Limited 2019

To the Editor:

The AML1-ETO fusion protein is produced by the t(8;21) translocation, which is the most common chromosomal abnormality in acute myeloid leukemia (AML). Although AML1-ETO alone is insufficient to cause leukemia, it is necessary for maintaining leukemia and therefore represents a therapeutic target. This notion has been supported by several lines of evidence: (i) transient suppression of AML1-ETO by small interfering RNA (siRNA) increases susceptibility of the leukemic cells to differentiation and delays leukemogenesis *in vivo* [1, 2]; (ii) in a mouse model harboring fully

developed leukemia, switching off AML1-ETO leads to leukemia regression [3]; (iii) in an AML1-ETO9a (AE9a)-driven leukemic mouse model, myeloid differentiation of leukemic cells triggered by panobinostat (an HDAC inhibitor) was attributed to AE9a degradation [4]; and (iv) mechanistic studies revealed that depletion of AML1-ETO in leukemic cells leads to a genome-wide epigenetic reprogramming and changes in transcription factor binding, resulting in myeloid differentiation and loss of leukemia maintenance [5].

We previously found that, in leukemic cells, AML1-ETO is stabilized and functions through the AML1-ETO-containing transcription factor complex (AETFC), which contains multiple transcription (co)factors that include AML1-ETO, CBF β , E proteins HEB and E2A, hematopoietic bHLH transcription factor LYL1, LIM domain protein LMO2 and its binding partner LDB1 [6]. These AETFC components mutually stabilize each other and cooperatively bind and regulate target genes, and AETFC integrity and proper conformation are essential for leukemogenesis [6]. Thus, destabilization of AETFC provides a strategy to target AML1-ETO. Notably, it has been generally proposed that the stability of a protein complex can

These authors contributed equally: Meng-Meng Zhang, Na Liu and Yuan-Liang Zhang

Data deposition: The RNA-seq and ChIP-seq data have been deposited in the Gene Expression Omnibus (GEO) database and are accessible through GEO series number GSE114642.

Supplementary information The online version of this article (<https://doi.org/10.1038/s41375-019-0398-8>) contains supplementary material, which is available to authorized users.

- ✉ Lan Wang
lwang@sibs.ac.cn
- ✉ Qiu-Hua Huang
hqh10632@rjh.com.cn
- ✉ Xiao-Jian Sun
xjsun@sibs.ac.cn

¹ State Key Laboratory of Medical Genomics, Shanghai Institute of Hematology, National Research Center for Translational Medicine, Ruijin Hospital, Shanghai Jiao Tong University School of Medicine, Shanghai, China

² CAS Key Laboratory of Tissue Microenvironment and Tumor, Shanghai Institute of Nutrition and Health, Shanghai Institutes for Biological Sciences, University of Chinese Academy of Sciences, Chinese Academy of Sciences, Shanghai, China

³ Liver Cancer Institute, Zhongshan Hospital, Fudan University, Key Laboratory of Carcinogenesis and Cancer Invasion, Ministry of Education, Key Laboratory of Epigenetics and Metabolism, Ministry of Science and Technology, and Institutes of Biomedical Sciences, Fudan University, Shanghai, China

⁴ Key Laboratory of Pediatric Hematology and Oncology, Ministry of Health, Department of Pediatric Hematology and Oncology, Shanghai Children's Medical Center, Shanghai Jiao Tong University School of Medicine, Shanghai, China

⁵ Department of Biochemistry and Molecular Biology, Department of Medicine, Sylvester Comprehensive Cancer Center, University of Miami Miller School of Medicine, Miami, FL, USA

⁶ Laboratory of Biochemistry and Molecular Biology, The Rockefeller University, New York, NY, USA

be reflected by its sensitivity to overexpression versus depletion of individual components [7]. First, many complexes can be destabilized by overexpression of individual components that, in a dosage-dependent manner, make promiscuous interactions that change the topology of the complex and thereby destabilize it. This mechanism, known as “dosage sensitivity”, is widely applicable to the regulation of protein functions in organisms ranging from yeast to human [8], including the interplay among the key transcription factors in hematopoiesis and leukemogenesis [9]. Second, other complexes show a lack of sensitivity (termed “robustness”) to component overexpression, likely because they possess strong multivalent interactions that cannot be altered by dosage increase, but can be perturbed by depletion, of individual components [10].

In this study, we investigated a means to destabilize AETFC, as well as the underlying mechanism. Following the principle described above, we first examined whether overexpression of AETFC components could affect the stability of the complex. In addition, several known interacting partners of AETFC components, including C/EBP α , TAL1, and ID1, were also analyzed. We transduced Kasumi-1 cells with retroviruses expressing HEB, E2A, E2-2, LDB1, LYL1, LMO2, C/EBP α , TAL1, or ID1 (Supplementary Figure S1a), and determined the protein levels of each AETFC component by immunoblot. The results showed that overexpression of the AETFC components failed to destabilize the complex (Fig. 1a). Thus, this result, in combination with our previous observation that knockdown of AETFC components in Kasumi-1 cells leads to degradation of the complex [6], reflects the “robustness” of AETFC. This result is also consistent with the extremely strong biochemical stability of AETFC that we previously established [6].

Unexpectedly, overexpression of C/EBP α dramatically decreased the protein levels of all AETFC components (Fig. 1a) and led to an accompanying inhibition of Kasumi-1 cell growth (Supplementary Figure S1b). To verify the loss-of-function of AETFC, we performed RNA-seq of the cells. Gene set enrichment analysis (GSEA) revealed that previously identified [6] effects of AETFC-loss on both the up and downregulated target genes tend to be mimicked by C/EBP α overexpression; this was confirmed by RT-qPCR analysis of representative genes (Fig. 1b). GSEA also revealed that the genes associated with myeloid differentiation are enriched, whereas those associated with hematopoietic stem cells are depleted, in the C/EBP α -activated genes (Supplementary Figure S2), consistent with the function of C/EBP α in myeloid differentiation [11]. We next employed the AE9a-driven leukemic mouse model to investigate whether C/EBP α overexpression could affect leukemogenesis. We observed that C/EBP α overexpression induces myeloid differentiation of the mouse leukemia cells and delays leukemogenesis in vivo, as indicated by an

increased frequency of CD11b⁺ cells and a significantly extended survival time of the mice (Fig. 1c). Thus, these results suggest that AETFC destabilization can be achieved by overexpression of C/EBP α , which is associated with cell differentiation and delayed leukemogenesis; however, the mechanism of how C/EBP α destabilizes AETFC is unclear.

While C/EBP α has been shown to physically interact with AML1-ETO [12], this interaction is relatively weak compared with the interactions among other factors (e.g., the interactions among AETFC components and the interactions of TAL1 and ID1 with E proteins), and thus is insufficient to mediate a “dosage sensitivity” effect that destabilizes AETFC [8]. We therefore examined whether C/EBP α overexpression can affect AETFC in other ways. Using RNA-seq and RT-qPCR, we found that C/EBP α overexpression leads to a significant decrease of *LYL1* mRNA, but not other AETFC component mRNAs (Fig. 2a). Our previous characterization of one-to-one interactions within AETFC revealed a central position of LYL1 (i.e., LYL1 interacts strongly with E proteins and LMO2 and weakly with AML1-ETO and LDB1) [6]. We thus speculated that loss of LYL1 could disrupt AETFC. To confirm this, we analyzed the integrity of AETFC in the presence and absence of LYL1 by co-immunoprecipitation (co-IP) assay, and we found that, if LYL1 is absent, LMO2 and LDB1 cannot be integrated into a complex with AML1-ETO and E proteins (Fig. 2b, i). Thus, LYL1 appears to act as a linker for the AML1-ETO-E proteins (AE-E) and the LMO2-LDB1 parts of AETFC. This mechanism was held valid for the endogenous AETFC, as knockdown of LYL1 in Kasumi-1 cells led to reduced amounts of LMO2 and LDB1 that bind to AML1-ETO (Supplementary Figure S3). An analysis of Kasumi-1 nuclear extract indicated that knockdown of LYL1 led to a dramatic degradation of LMO2 and LDB1, as well as decreased HEB and E2A (Fig. 2b, ii); AML1-ETO was lagged behind in this degradation process likely due to a different degradation mechanism for AML1-ETO relative to other AETFC components. In contrast, knockdown of TAL1, a homologue of LYL1, did not show such an AETFC destabilization effect (Fig. 2b, ii). Conversely, overexpression of LYL1 in the C/EBP α -overexpressed Kasumi-1 cells rescued AETFC stability, and the extent of restoration of different AETFC components correlates with the interaction strength and spatial distance between these components and LYL1 (Fig. 2b, iii). Taken together, these results suggest that downregulation of LYL1 by C/EBP α contributes to the AETFC destabilization.

To investigate whether LYL1 is directly regulated by C/EBP α and to gain a genome-wide view of C/EBP α binding, we performed a ChIP-seq analysis of the overexpressed C/EBP α in Kasumi-1 cells. The results showed that C/EBP α directly binds to an \sim –1 kb region of the *LYL1* locus

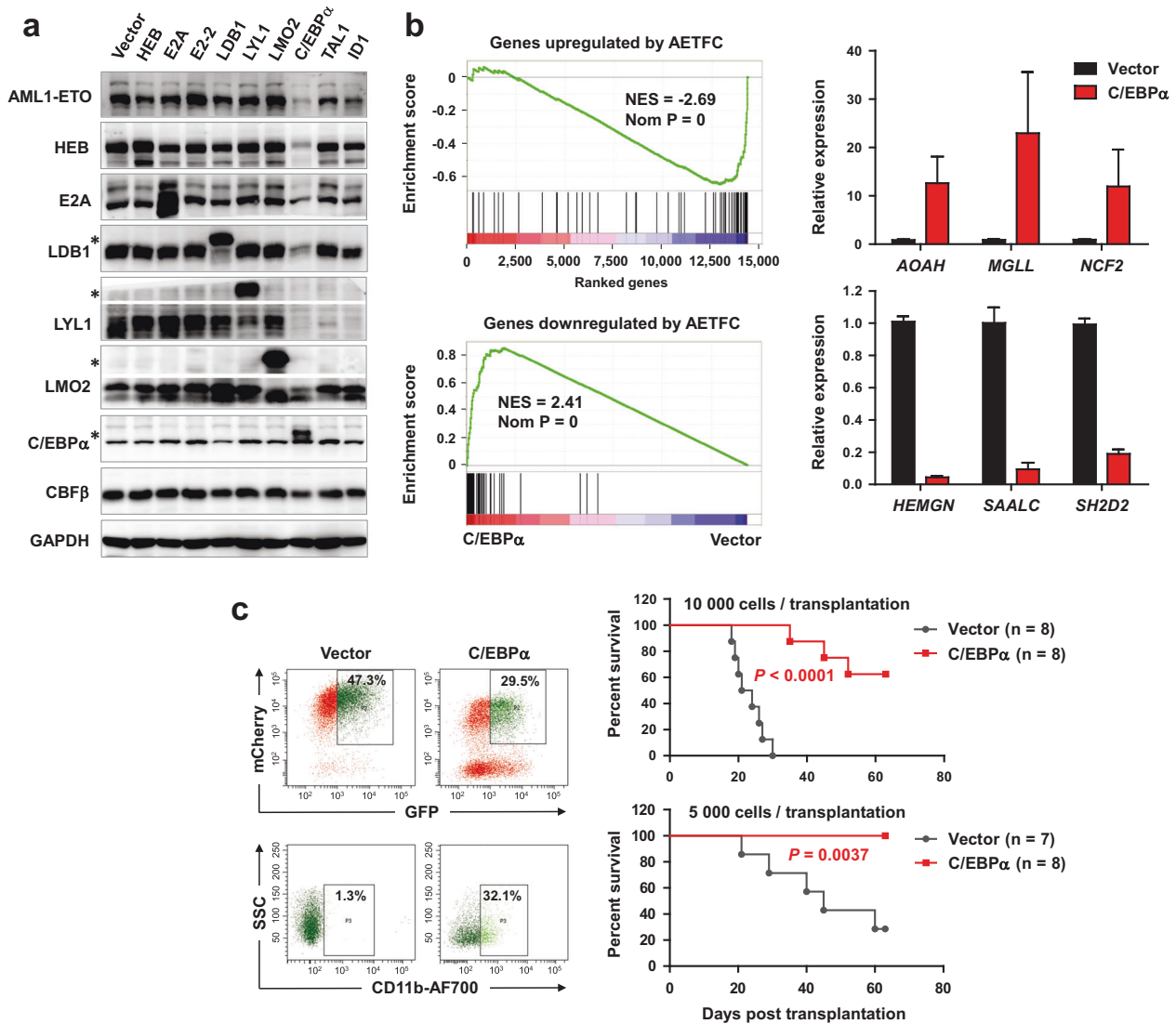
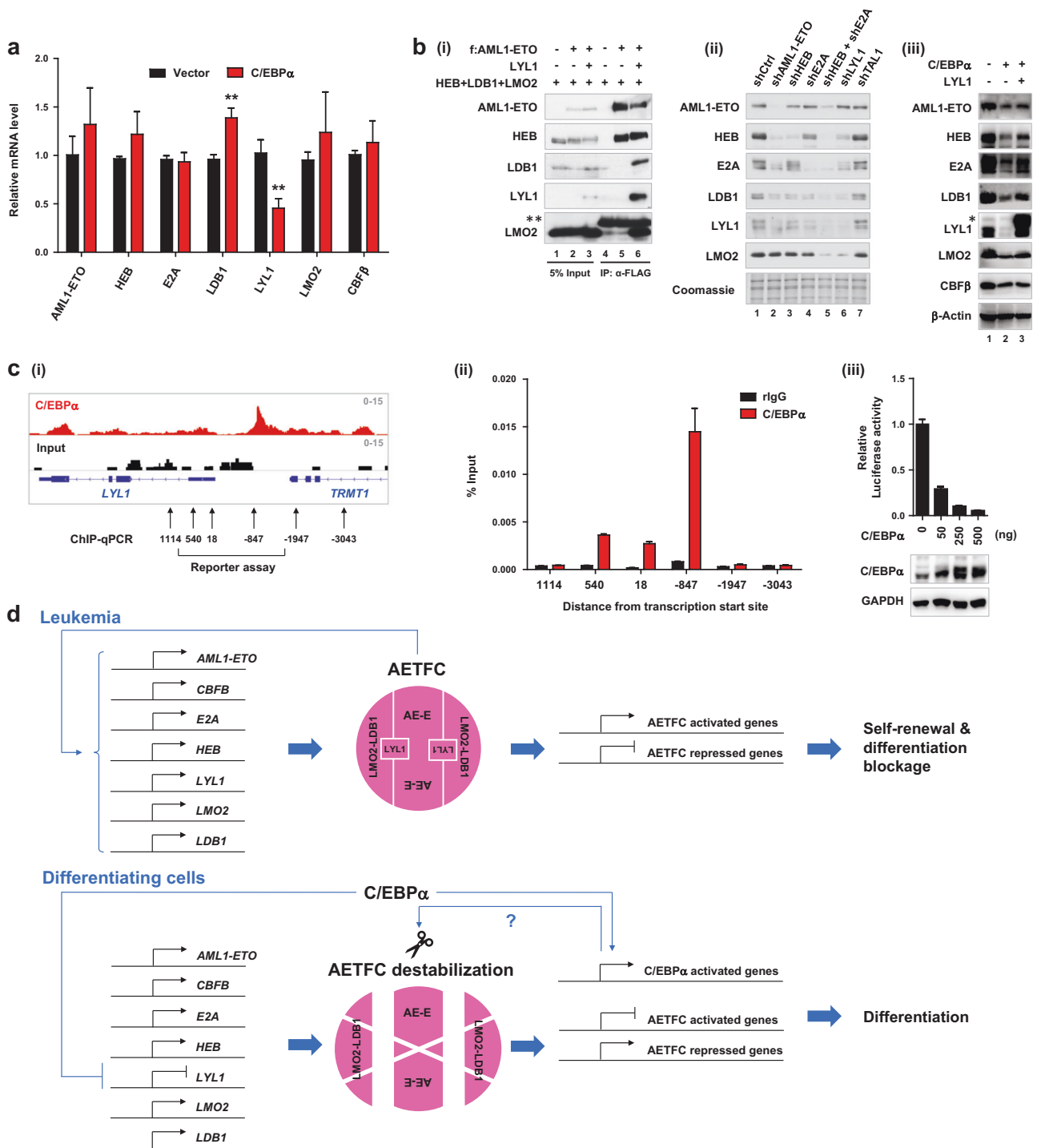


Fig. 1 Destabilization of AETFC by overexpression of C/EBP α and its role in cell differentiation and leukemogenesis. **a** Immunoblot analysis of AETFC components in Kasumi-1 cells upon overexpression of indicated proteins. Note that overexpression of C/EBP α , but not the AETFC components, leads to a decrease of AETFC components. Overexpression of TAL1 or ID1 only decreases LYL1, suggesting different mechanism(s) relative to C/EBP α . Asterisks denote the larger sizes of exogenous tagged proteins relative to the endogenous ones. **b** RNA-seq and GSEA (left) and RT-qPCR (right) analyses of Kasumi-1 cells expressing C/EBP α , showing that overexpression of C/EBP α

(Fig. 2c, i), which was confirmed by ChIP-qPCR (Fig. 2c, ii). Recently published ChIP-seq data also indicated that this region is physiologically bound by endogenous C/EBP α in myeloid cell lines (Supplementary Figure S4). Interestingly, this -1 kb region is distinct from the previously reported promoter region (within 542 bp upstream of *LYL1* transcription start site) bound by ETS and GATA factors [13]. C/EBP α is known mostly as a transcriptional activator and, according to our RNA-seq data, overexpressed C/EBP α in Kasumi-1 cells activates more genes relative to repressed

genes (Supplementary Figure S5a). However, it has also been established that C/EBP α can repress genes [14] (e.g., *MYC*, *MYB*, and *GATA2*), and we observed direct binding and downregulation of these genes by C/EBP α in Kasumi-1 cells (Supplementary Figure S5b and c). To validate that C/EBP α directly represses *LYL1* transcription, we performed a luciferase reporter assay and observed that the transcriptional activity of the *LYL1* promoter is decreased upon C/EBP α overexpression in a dosage-dependent manner (Fig. 2c, iii). Furthermore, GSEA revealed a strong



correlation between the genes upregulated by C/EBPα and those derepressed by LYL1 knockdown (Supplementary Figure S6a), suggesting that repression of LYL1 to some degree recapitulates the effect of C/EBPα overexpression.

We next investigated whether LYL1 repression contributes to leukemic cell differentiation. We simultaneously overexpressed LYL1 and C/EBPα in Kasumi-1 cells and assessed their differentiation. The results showed that the

LYL1 overexpression reduces the number of C/EBPα-induced CD11b⁺ cells (Supplementary Figure S6b). Furthermore, we observed that knockdown of LYL1 enhances the ability of Kasumi-1 cells to differentiate upon induction by Vitamin D3, which otherwise shows very subtle effect on the cells (Supplementary Figure S6c). These results suggest that the LYL1 depletion can release the differentiation blockage in leukemic cells, although it is

Fig. 2 Direct repression of the core AETFC component LYL1 by C/EBP α , leading to disruption of AETFC. **a** RT-qPCR analysis of mRNA levels of AETFC components in Kasumi-1 cells upon C/EBP α overexpression. Note that only *LYL1* mRNA is decreased. Data are presented as mean \pm SD of three independent experiments with triplicates each time; ** $P < 0.01$; two-tailed *t*-test. **b** The role of LYL1 in AETFC stabilization. (i) Co-IP analysis of AETFC integrity in 293 T cells co-transfected with FLAG-tagged (f): AML1-ETO and indicated components, showing that LYL1 is required for interaction between the AML1-ETO-HEB and the LMO2-LDB1 parts of AETFC. Double asterisk denotes immunoglobulin signal. (ii) Immunoblot analysis of AETFC in Kasumi-1 cell nuclear extract upon knockdown of indicated components, showing that knockdown of LYL1 leads to AETFC degradation. Nuclear extract was used in this assay to exclude any cytoplasmic AETFC components. Also shown are knockdowns of E proteins and TAL1 as positive and negative controls, respectively. (iii) Rescue of AETFC stability by overexpression of LYL1 in the C/EBP α -overexpressing Kasumi-1 cells. Note that the stronger LYL1-interacting AETFC component shows a better restoration extent, suggesting a possible stepwise restoration of the complex. Asterisk denotes the exogenous tagged LYL1. **c** C/EBP α directly represses the transcription of the *LYL1* gene. (i) ChIP-seq analysis of overexpressed C/EBP α in Kasumi-1 cells, showing its binding to the *LYL1* locus. Arrows with numbers and bracket denote the regions selected for ChIP-qPCR and promoter reporter assays. (ii) ChIP-qPCR validation of C/EBP α binding to the indicated regions in the *LYL1* locus. An anti-C/EBP α antibody was used in this ChIP experiment, and a rabbit immunoglobulin G (rIgG) was used as a negative control. (iii) Luciferase reporter assay showing repression of the *LYL1* promoter by C/EBP α . A dosage-dependent effect of C/EBP α was revealed by transfection of different amounts of C/EBP α plasmid and immunoblot analysis of protein levels. **d** A working model. In leukemic cells, the robustness of AETFC is maintained by both the strong multivalent interactions within AETFC and a positive feedback loop in the transcriptional network (upper). Overexpression of C/EBP α specifically and directly represses LYL1, and thereby breaks the connection between the AML1-ETO-E (AE-E) and the LMO2-LDB1 parts of AETFC, leading to AETFC destabilization (lower). Potentially also involving other C/EBP α -activated genes (denoted by a question mark), these molecular events trigger degradation of AETFC/AML1-ETO and differentiation of leukemic cells

insufficient to induce a complete differentiation as does C/EBP α (Supplementary Figure S6c). This insufficiency is likely because C/EBP α activates many genes required for myeloid differentiation, while LYL1 depletion and AETFC destabilization can release the repression of some genes but cannot fully activate them.

In summary, our study first demonstrated an AETFC “robustness” in leukemic cells, which confer on the complex a resistance to a destabilization strategy based on overexpression of AETFC components. However, we found that overexpression of C/EBP α can destabilize AETFC by direct repression of the core component LYL1 at the transcriptional level, and that the depletion of LYL1 causes AETFC disruption that increases susceptibility of the leukemic cells to differentiation (Fig. 2d). The important role of C/EBP α in t(8;21) leukemia development and treatment has been established [11] and recently re-emphasized by several interesting studies showing that depletion of AML1-

ETO activates a C/EBP α -dominated transcriptional network [15] and that C/EBP α overrides the repressive activity of AML1-ETO [16]. Our studies provide a new mechanism by which C/EBP α can destabilize AETFC, suggesting restoration of C/EBP α as a strategy for leukemia therapy, and further identifying LYL1 as a new therapeutic target in t(8;21) leukemia.

Acknowledgements This work was supported by the National Key Research and Development Plan of China 2018YFA0107802 (X-JS) and 2018YFA0107202 (LW), the Chinese Academy of Sciences (CAS) Bureau of Frontier Sciences and Education Program QYZDBSSW-SMC027 (L.W.), the National Natural Science Foundation of China (NSFC) General Program 81470316, 81670094 (X-JS), 81670149 (Q-HH), 81470334, 81670122 (LW), 81270623 (SS) and Youth Program 81500080 (Y-LZ), the NSFC Excellent Young Scholar Program 81622003 (LW), the Chinese National Key Basic Research Project 2013CB966801 (X-JS), the National Key Research and Development Plan of China 2016YFC0902202 (LW), the National Institutes of Health (NIH) of USA R01 grants CA163086, CA178765 (RGR) and CA166835 (SDN), the Shanghai Municipal Education Commission-Gaofeng Clinical Medicine Grant 20152506 (X-JS), the CAS Bureau of Major R&D Program XDA12020376 (LW), the fourth round of Three Year Public Health Action Plan GWIV-25 (SS), the Shanghai Municipal Science and Technology Major Project 2017SHZDZX01 (FL), the 111 Project B17029 (X-JS, RGR, and S-JC), and the Samuel Waxman Cancer Research Foundation. X-JS and LW were supported by the 1000 Talents Program for Young Scholars. We thank Y. Zhai, X. Miao, S. Yan, Y. Chen, K. Wang and Y. Wang at the Shanghai Institute of Nutrition and Health core facilities for technical support.

Compliance with ethical standards

Conflict of interest The authors declare that they have no conflict of interest.

Publisher's note: Springer Nature remains neutral with regard to jurisdictional claims in published maps and institutional affiliations.

References

- Heidenreich O, Krauter J, Riehle H, Hadwiger P, John M, Heil G, et al. AML1/MTG8 oncogene suppression by small interfering RNAs supports myeloid differentiation of t(8;21)-positive leukemic cells. *Blood*. 2003;101:3157–63.
- Martinez Soria N, Tussiwand R, Ziegler P, Manz MG, Heidenreich O. Transient depletion of RUNX1/RUNX1T1 by RNA interference delays tumour formation in vivo. *Leukemia*. 2009;23:188–90.
- Cabezas-Wallscheid N, Eichwald V, de Graaf J, Lower M, Lehr HA, Kreft A, et al. Instruction of haematopoietic lineage choices, evolution of transcriptional landscapes and cancer stem cell hierarchies derived from an AML1-ETO mouse model. *EMBO Mol Med*. 2013;5:1804–20.
- Bots M, Verbrugge I, Martin BP, Salmon JM, Ghisi M, Baker A, et al. Differentiation therapy for the treatment of t(8;21) acute myeloid leukemia using histone deacetylase inhibitors. *Blood*. 2014;123:1341–52.
- Ptasinska A, Assi SA, Mannari D, James SR, Williamson D, Dunne J, et al. Depletion of RUNX1/ETO in t(8;21) AML cells

- leads to genome-wide changes in chromatin structure and transcription factor binding. *Leukemia*. 2012;26:1829–41.
6. Sun XJ, Wang Z, Wang L, Jiang Y, Kost N, Soong TD, et al. A stable transcription factor complex nucleated by oligomeric AML1-ETO controls leukaemogenesis. *Nature*. 2013;500:93–7.
 7. Marcotte EM, Tschansky M. Disorder, promiscuity, and toxic partnerships. *Cell*. 2009;138:16–8.
 8. Vavouri T, Semple JI, Garcia-Verdugo R, Lehner B. Intrinsic protein disorder and interaction promiscuity are widely associated with dosage sensitivity. *Cell*. 2009;138:198–208.
 9. Rosenbauer F, Tenen DG. Transcription factors in myeloid development: balancing differentiation with transformation. *Nat Rev Immunol*. 2007;7:105–17.
 10. Semple JI, Vavouri T, Lehner B. A simple principle concerning the robustness of protein complex activity to changes in gene expression. *BMC Syst Biol*. 2008;2:1.
 11. Pabst T, Mueller BU, Harakawa N, Schoch C, Haferlach T, Behre G, et al. AML1-ETO downregulates the granulocytic differentiation factor C/EBPalpha in t(8;21) myeloid leukemia. *Nat Med*. 2001;7:444–51.
 12. Westendorf JJ, Yamamoto CM, Lenny N, Downing JR, Selsted ME, Hiebert SW. The t(8;21) fusion product, AML-1-ETO, associates with C/EBP-alpha, inhibits C/EBP-alpha-dependent transcription, and blocks granulocytic differentiation. *Mol Cell Biol*. 1998;18:322–33.
 13. Chan WY, Follows GA, Lacaud G, Pimanda JE, Landry JR, Kinston S, et al. The paralogous hematopoietic regulators Lyl1 and Scl are coregulated by Ets and GATA factors, but Lyl1 cannot rescue the early Scl^{-/-} phenotype. *Blood*. 2007;109:1908–16.
 14. Ohlsson E, Schuster MB, Hasemann M, Porse BT. The multifaceted functions of C/EBPalpha in normal and malignant haematopoiesis. *Leukemia*. 2016;30:767–75.
 15. Ptasinska A, Assi SA, Martinez-Soria N, Imperato MR, Piper J, Cauchy P, et al. Identification of a dynamic core transcriptional network in t(8;21) AML that regulates differentiation block and self-renewal. *Cell Rep*. 2014;8:1974–88.
 16. Loke J, Chin PS, Keane P, Pickin A, Assi SA, Ptasinska A, et al. C/EBPalpha overrides epigenetic reprogramming by oncogenic transcription factors in acute myeloid leukemia. *Blood Adv*. 2018;2:271–84.

Leukemia (2019) 33:1827–1832

<https://doi.org/10.1038/s41375-019-0399-7>

Acute myeloid leukemia

GATA1 epigenetic deregulation contributes to the development of AML with NPM1 and FLT3-ITD cooperating mutations

Paolo Sportoletti¹ · Letizia Celani¹ · Emanuela Varasano¹ · Roberta Rossi¹ · Daniele Sorcini¹ · Chiara Rompietti¹ · Francesca Strozzi¹ · Beatrice Del Papa¹ · Valerio Guarente¹ · Giulio Spinozzi¹ · Debora Cecchini¹ · Oxana Bereshchenko² · Torsten Haferlach³ · Maria Paola Martelli¹ · Franca Falzetti¹ · Brunangelo Falini¹

Received: 19 September 2018 / Revised: 30 December 2018 / Accepted: 21 January 2019 / Published online: 12 February 2019

© The Author(s) 2019. This article is published with open access

Supplementary information The online version of this article (<https://doi.org/10.1038/s41375-019-0399-7>) contains supplementary material, which is available to authorized users.

✉ Paolo Sportoletti
paolo.sportoletti@unipg.it

✉ Brunangelo Falini
brunangelo.falini@unipg.it

¹ Centro di Ricerca Emato-Oncologica (CREO), University of Perugia, Perugia 06132, Italy

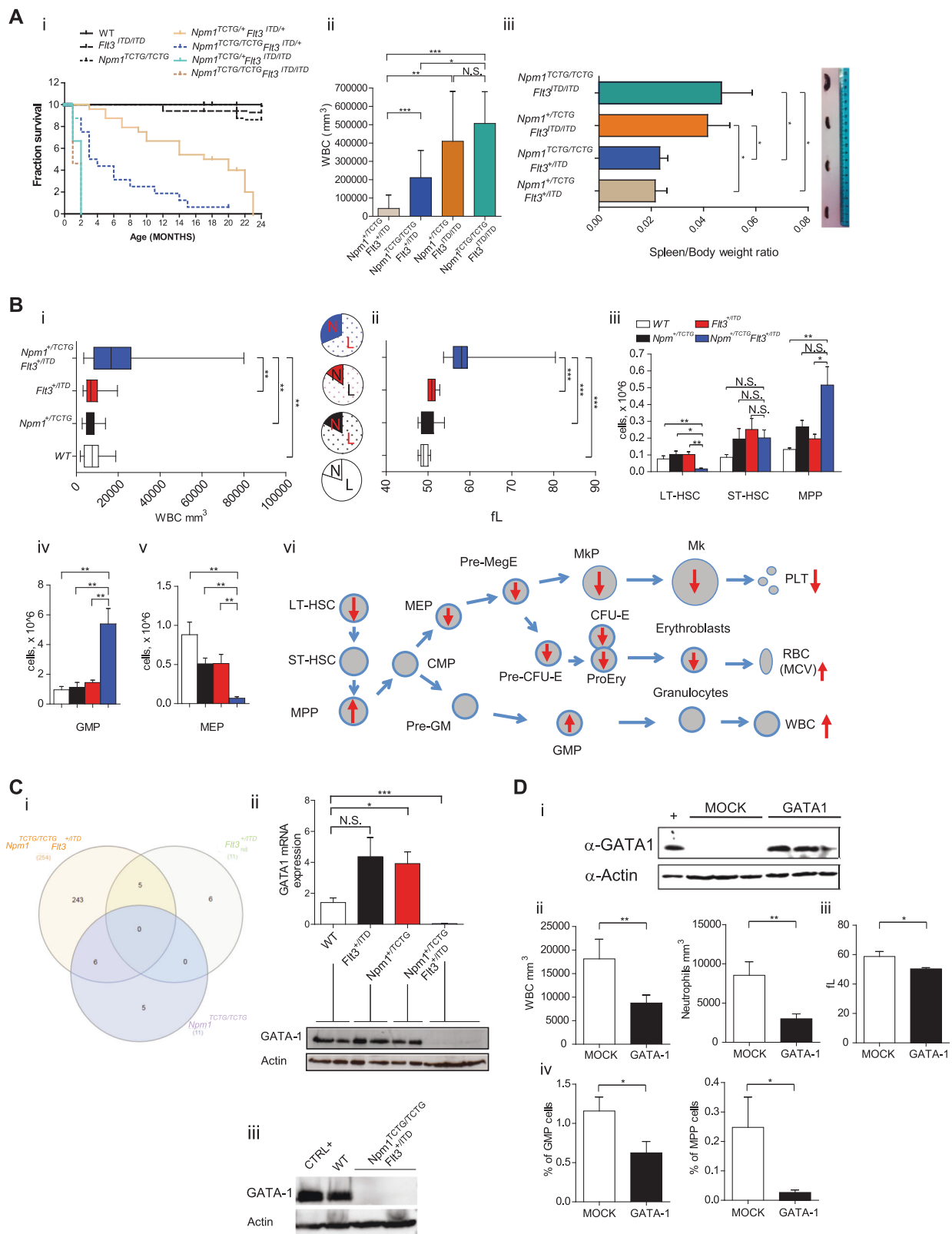
² Section of Pharmacology, Toxicology and Chemotherapy, University of Perugia, Perugia 06132, Italy

³ MLL Munich Leukemia Laboratory, Munich 81377, Germany

To the Editor:

About 20 recurrently mutated genes are known to be involved in the molecular pathogenesis of acute myeloid leukemia (AML) [1]. Among them, *Nucleophosmin* (*NPM1*) and *FLT3*-ITD mutations frequently occur together in adults with AML [2], suggesting cooperative leukemogenesis. To date, the molecular consequences of these cooperative genetic alterations in AML are still elusive.

To address this issue, we crossed *Npm1* and *Flt3-ITD* mutant mice demonstrating the onset of lethal AML (Fig. 1a and Figure S1). Interestingly, the cumulative mutant allele burden influenced the leukemic phenotype, penetrance and latency. *NPM1*/*Flt3*-ITD double heterozygous mice (*Npm1*^{+TCTG};*Flt3*^{+ITD}) displayed a significantly reduced overall survival compared to single mutant or wild-type mice. Survival was further reduced in mice with two *NPM1* mutant alleles and one *Flt3*-ITD allele (*Npm1*^{TCTG/TCTG};*Flt3*^{+ITD}).



Interestingly, *Fli3*-ITD homozygous mice (*Npm1*^{+TCTG}; *Fli3*^{ITD/ITD} and *Npm1*^{TCTG/TCTG}; *Fli3*^{ITD/ITD}) showed the higher white blood cell (WBC) counts, a significant spleen

enlargement (Fig. 1a ii-iii) and developed AML rapidly regardless of *NPM1* mutation dosage, suggesting that in the context of a high *FLT3* kinase activity even small *NPM1*

◀ **Fig. 1** Lethal acute myeloid leukemia (AML) in *Npm1/Flt3-ITD* mice is preceded by changes in myeloid and erythroid cells associated with GATA1 deregulation. **a** (i) Kaplan–Meier plot of mouse survival according to the indicated genotypes ($n = 8$ to 24 per genotype); *Npm1^{+TCTG};Flt3^{+ITD}* mice display a median survival of 18.5 months versus 21 months of *Npm1^{+TCTG}* or *Flt3^{+ITD}* mice or 22.5 months of wild-type controls ($p < 0.0001$, logrank test). (ii) Changes in white blood cell (WBC) counts of *Npm1^{+TCTG};Flt3^{+ITD/ITD}* ($n = 3$), *Npm1^{TCTG/TCTG};Flt3^{ITD/ITD}* ($n = 3$), *Npm1^{+TCTG};Flt3^{+ITD}* ($n = 6$) and *Npm1^{TCTG/TCTG};Flt3^{+ITD}* ($n = 9$) mice. (iii) Spleen weight to total body weight ratio in the indicated genotypes. Spleen ratio in *Npm1^{+TCTG};Flt3^{+ITD/ITD}* ($n = 3$) and *Npm1^{TCTG/TCTG};Flt3^{+ITD/ITD}* ($n = 4$) mice was two fold greater than in *Npm1^{+TCTG};Flt3^{+ITD}* ($n = 5$) and *Npm1^{TCTG/TCTG};Flt3^{+ITD}* ($n = 18$) leukemic mice (0.041 ± 0.014 and 0.046 ± 0.023 vs 0.017 ± 0.012 and 0.025 ± 0.016 $p < 0.001$ by one-way analysis of variance (ANOVA) analysis). **b** (i) Significant differences in WBC count in *Npm1^{+TCTG};Flt3^{+ITD}* compared to *Npm1^{+TCTG};Flt3^{+/+}*, *Npm1^{+/+};Flt3^{+ITD}* and *Npm1^{+/+};Flt3^{+/+}* littermate groups ($n = 12$ to 20 per genotype); pie charts show neutrophils (N) and lymphocytes (L) percentages. (ii) Mean corpuscular volume (MCV) values in preleukemic mice ($n = 12$ to 20 per genotype). (iii–v) Flow-cytometric analysis of bone marrow stem and progenitor cell compartment sizes, including long-term hematopoietic stem cells (LT-HSCs; $\text{lin}^- \text{Sca-1}^+ \text{c-kit}^+ \text{CD34}^- \text{Flt3}^-$), short-term HSCs (ST-HSCs; $\text{lin}^- \text{Sca-1}^+ \text{c-kit}^+ \text{CD34}^+ \text{Flt3}^-$), multipotent progenitors (MPPs; $\text{lin}^- \text{Sca-1}^+ \text{c-kit}^+ \text{CD34}^+ \text{Flt3}^+$), granulocyte/monocyte progenitors (GMPs $\text{Lin}^- \text{Sca-1}^- \text{cKit}^+ \text{CD34}^+ \text{FcγRII/III}^{\text{hi}}$) and common megakaryocyte-erythroid progenitor (MEP; $\text{Lin}^- \text{Sca-1}^- \text{cKit}^+ \text{CD34}^- \text{FcγRII/III}^{\text{lo}}$) populations ($n = 4$ to 10 per genotype). (vi) Summary of hemopoietic changes in *Npm1^{+TCTG};Flt3^{+ITD}* mice. **c** (i) Overlap of differently gene expression profiling (GEP) of *Npm1^{TCTG/TCTG};Flt3^{+/+}*, *Npm1^{+/+};Flt3^{+ITD}* and *Npm1^{TCTG/TCTG};Flt3^{+ITD}* compared to *Npm1^{+/+};Flt3^{+/+}* ($n = 3$ mice for each genotype). (ii) GATA1 messenger RNA (mRNA) and protein expression in the bone marrow (BM) of the indicated genotypes. (iii) GATA1 protein expression in lineage-depleted BM cells from the indicated genotypes. **d** (i) Enforced expression of GATA1 protein in the BM of mice transplanted with *Npm1^{+TCTG};Flt3^{+ITD}* LSK ($n = 4$ to 12) infected with an inducible GATA1 lentiviral system and killed 2 months after transplantation. (ii, iii) Significant differences in WBC counts, neutrophils and MCV values in the peripheral blood (PB) of GATA1-rescued mice. (iv) Frequency of MPP and GMP populations in MOCK ($n = 10$) and GATA1 ($n = 16$) infected mice. Data represent the mean \pm SD. N.S. not significant; * $p < 0.05$, ** $p < 0.01$, *** $p < 0.001$; unpaired t -test with Welch's correction

mutant levels are leukemogenic. This supports a direct oncogenic effect of the NPM1 mutant, beside the haploinsufficient tumor suppressor effects of the concomitant loss of one *NPM1* allele [3, 4]. Additionally, our data are in line with the clinical observation that normal karyotype AML with high *FLT3-ITD* levels have a poor outcome [5].

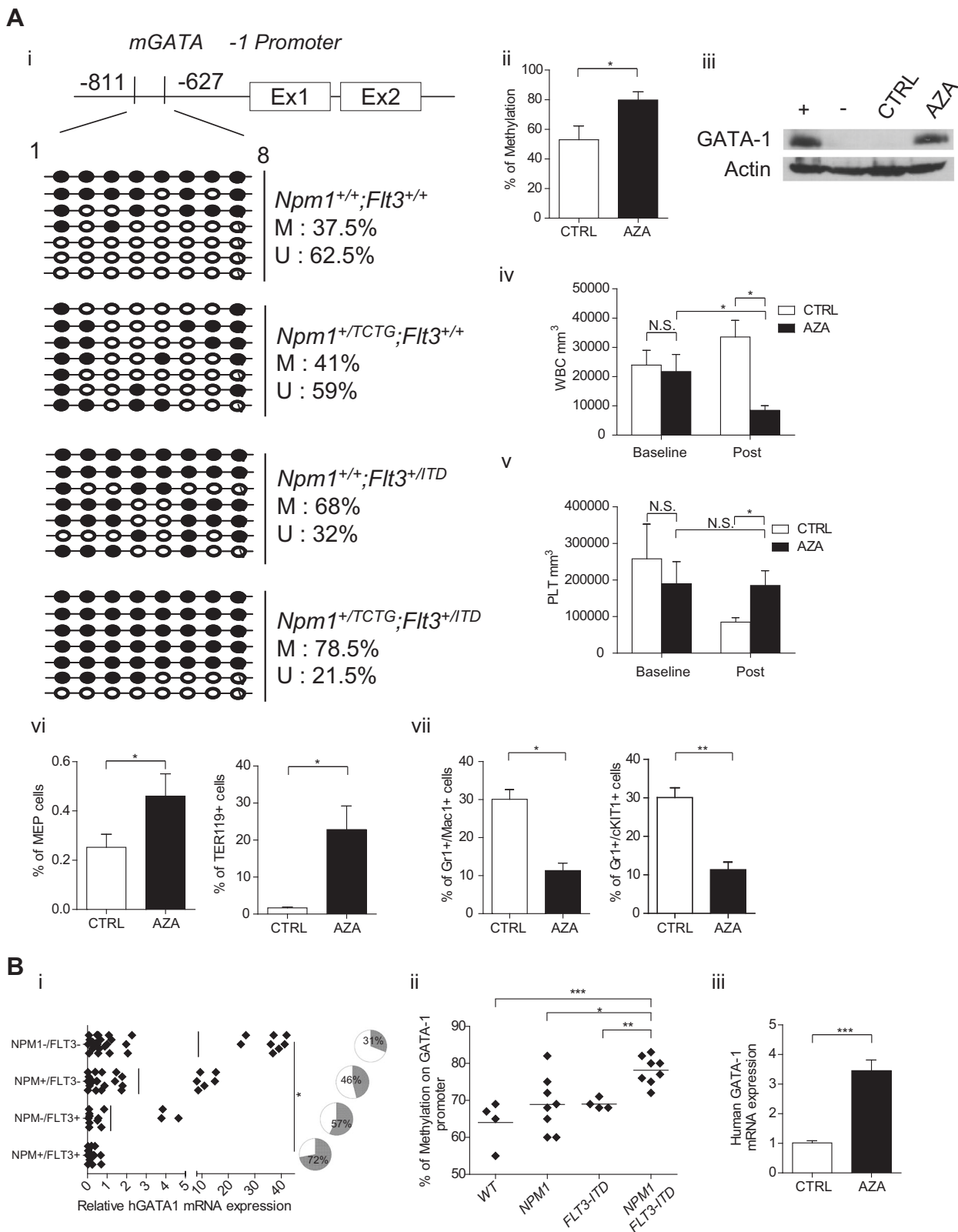
The analysis of the *Npm1^{+TCTG};Flt3^{+ITD}* genotype, which is characterized by a longer AML latency, demonstrated changes in the myeloid and erythroid cells before leukemia onset. WBC counts and mean corpuscular volume (MCV) were significantly higher in *Npm1^{+TCTG};Flt3^{+ITD}* mice than in wild-type, *Npm1^{+TCTG}* and *Flt3^{+ITD}* groups (Fig. 1b i-ii). Flow cytometry analysis of bone marrow (BM) populations showed that leukocytosis was associated to reduced long-term hematopoietic stem cells (HSCs), significant expansion of

multipotent progenitor (MPP) cells and a 6.1-fold increase of granulocyte/monocyte progenitors (GMPs) (Fig. 1b iii-iv). *Npm1^{+TCTG};Flt3^{+ITD}* mice had decreased number of immature and recirculating B-cell BM populations (Figure S2). Erythrocyte changes reflected a significant reduction in the corresponding BM populations at different differentiation stages including myelo-erythroid progenitors (MEP), pre-megakaryocyte-erythrocyte progenitors (PreMegE), pre-colony forming unit-erythroid (pre-CFU-E), CFU-E and proerythroblasts (proEry) that resulted almost absent (Fig. 1b v-vi and Figure S3). In physiological hematopoiesis, FLT3 up-regulation is important in sustaining MPP and GMP but not MEP potential [6]. In *Npm1^{+TCTG};Flt3^{+ITD}* mice, constitutive Flt3-ITD signaling boosts the myeloid bias and influences the megakaryocyte/erythroid lineage fates, strongly suggesting the capacity of the NPM1 mutant to synergize with a FLT3 activity. These findings appear to define the cellular background for the acquisition of additional events for AML onset.

Comparative gene expression profiling (GEP) studies on total BM revealed a large number of differentially expressed genes in *Npm1^{TCTG/TCTG};Flt3^{+ITD}* leukemic mice compared to *Flt3^{+ITD}*, *Npm1^{TCTG/TCTG}* and wild-type groups. A total of 254 genes were differentially expressed in *Npm1^{TCTG/TCTG};Flt3^{+ITD}* mice compared to wild-type littermates (42 up-regulated; 214 down regulated) (Table S1). Interestingly, when compared with wild-type, there were 243 transcripts whose expression was changed only in *Npm1^{TCTG/TCTG};Flt3^{+ITD}* cells (Fig. 1c i). There were no transcripts commonly altered in all pairwise comparisons. *Hoxa9* scored as one of the most up-regulated genes in *Npm1^{TCTG/TCTG};Flt3^{+ITD}* mice, a characteristic hallmark of *NPM1*-driven leukemia. Similar findings were present in mice with early-stage AML.

Pathway analysis showed different changes when comparing *Npm1^{TCTG/TCTG};Flt3^{+ITD}* to wild-type mice. Among these, we found pathways involved in hematopoietic cell lineage development, the B-cell receptor signaling and the immunoregulatory interactions between lymphoid and non-lymphoid cells. Additionally, *Npm1^{TCTG/TCTG};Flt3^{+ITD}* BM samples displayed a significant deregulation of factors involved in megakaryocyte development and platelet production. Interestingly, several genes associated with this pathway were linked to a GATA transcriptional signature, including GATA1, Zfp1, Rac1 and Ehd2. The latter showed a significant downregulation, with GATA1 displaying the lower levels (Figure S4). A similar expression signature was present in lineage-depleted BM cells used to exclude biases related to the different cellular composition of leukemic versus wild-type mice (Figure S5). In this context, we found a higher number of deregulated GATA gene family members including GATA1, GATA2 and GATA3.

Results of GEPs and the presence of alterations in erythropoiesis before AML development prompted us to focus



on GATA1, the master regulator of erythroid differentiation. Notably, BM changes in *Npm1*^{+/*TCTG*};*Flt3*^{+/*ITD*} mice were accompanied by a dramatic reduction of GATA1 messenger

RNA (mRNA) and complete loss and substantial down-regulation of protein expression in both total or lineage-depleted BM (Fig. 1c ii-iii). The extent of GATA1

◀ **Fig. 2** Decreased GATA1 expression levels in human and mouse *NPM1/FLT3-ITD* mutated acute myeloid leukemia (AML) depends on promoter methylation. **a** (i) Analysis of DNA methylation at the mouse *GATA1* locus by sequencing of PCR clones derived from sodium bisulfite-treated mouse genomic DNA extracted from the bone marrow (BM). Each row of circles represents the sequence of an individual clone; open circles indicate unmethylated CpG sites and closed circles indicate methylated CpG sites. (ii) Methylation status of the *GATA1* promoter as determined by the Methylight assay. (iii) *GATA1* protein expression in the BM of Aza-treated mice ($n = 5$). (iv, v) Changes in white blood cell (WBC) and platelet (PLT) counts of *Npm1^{+TCTG};Flt3^{+ITD}* mice treated with Aza ($n = 5$ to 10 per treatment group). (vi) Frequencies of MEP and Ter119 cells in the BM of Aza-treated mice ($n = 5$ to 12 per treatment group). (vii) Frequencies of Gr1+cKit+ immature and Gr1+Mac1+ mature myeloid cells in the spleen of untreated vs 5-Aza-treated leukemic mice ($n = 5$). **b** (i) *GATA1* mRNA average expression in AML patients with *NPM1/FLT3-ITD* mutation compared to unmutated, *NPM1* and *FLT3-ITD* single mutant ($p < 0.05$ comparing all the groups); pie charts indicate the percentage of patients with *GATA1* expression below the median in the indicated mutation group. (ii) *GATA1* promoter methylation frequency in AML patients with *NPM1/FLT3-ITD* mutation ($n = 8$) as compared to unmutated ($n = 4$), *NPM1* ($n = 8$) and *FLT3-ITD* ($n = 4$) single mutant. (iii) *GATA1* mRNA levels in the BM of human AML patients ($n = 3$) before and after in vivo Aza treatment. N.S. not significant; * $p < 0.05$, ** $p < 0.01$; *** $p < 0.001$; unpaired *t*-test with Welch's correction

deregulation correlated with the degree of the myeloid phenotypic changes (Figure S6). In vivo restoration of *GATA1* expression in *Npm1^{+TCTG};Flt3^{+ITD}* Lin⁻Sca-1⁺cKit⁺ cells using a conditional lentiviral system (Fig. 1d i and Figure S7A) rescued most of the preleukemic phenotype which included a significant reduction of WBC and neutrophils in peripheral blood (PB) and a decrease in percentage of MPP and GMP (Fig. 1d ii,iv and Figure S7B). Interestingly, *GATA1* re-expression also led to a rescue of macrocytosis with a significant reduction of the MCV values from 58.7 to 50.2 fL (Fig. 1d iii). Moreover, spleens from *GATA1*-rescued mice showed a decrease in size and a reduction of myeloid-infiltrating cells compared to controls (Figure S7C). Collectively, these findings provide evidence that deregulation of *GATA1* plays a key role in the hemopoietic changes preceding AML in *Npm1^{+TCTG};Flt3^{+ITD}* mice. This is consistent with the concept that in blood cell precursors, *GATA1* is necessary for erythroid lineage differentiation and antagonizes the activity of myeloid transcription factors [7].

Our findings are consistent with the observation that *GATA1* heterozygous knock-out female mice frequently develop a myeloproliferative disorder with a splenic accumulation of proerythroblasts and megakaryocytes, anemia and thrombocytopenia [7]. Moreover, recurrent *GATA1* mutations abrogating the expression of the full-length *GATA1* have been found in myeloid proliferations related to Down syndrome, including transient abnormal myelopoiesis and megakaryoblastic AMLs [8]. Interestingly, *FLT3-ITD* mutations were more frequent in AML patients

who lacked *GATA1* expression [9] and even *IDH*-mutated AML patients displayed a distinct methylation signature, including the aberrant hypermethylation of *GATA1/2* gene promoter [10].

Proteasome inhibition of *Npm1^{+TCTG};Flt3^{+ITD}* BM cells in vitro did not rescue *GATA1* protein expression (Figure S8A), suggesting that *NPM1* and *Flt3-ITD* mutations regulate *GATA1* transcription. Thus, we explored changes in the methylation status of the *GATA1* promoter region (from -811 to -627 bp) and observed dense DNA methylation in *Npm1^{+TCTG};Flt3^{+ITD}* samples (Fig. 2a i-ii). To support *GATA1* epigenetic silencing as a mechanism favoring AML, we treated *Npm1^{+TCTG};Flt3^{+ITD}* mice with the DNA methyltransferase inhibitor 5-aza-deoxycytidine (5-Aza-dC). This resulted in the reactivation of *GATA1* expression in BM (Fig. 2a iii and Figure S8B), normalization of leukocytosis and prevention of a drop in platelet counts (Fig. 2a iv-v). Although 5-Aza-dC treatment had no impact on MCV, both MEP and Ter119 cells were significantly expanded in treated animals (Fig. 2a vi). Flow cytometry of spleen demonstrated a significant reduction of both mature and immature myeloid cells in 5-Aza-dC-treated mice (Fig. 2a vii). Our findings are reminiscent of the differential methylation of *GATA* target genes previously reported in AML mouse models combining *FLT3-ITD* to either *IDH* mutants [11] or *TET2* loss [12]. The higher 5'-*GATA1* methylation in *Npm1^{+TCTG};Flt3^{+ITD}* mice points to a gene dose effect for *GATA1* during leukemogenesis being finely tuned by CpG methylation. This suggests that *NPM1* alterations may contribute to epigenetic modifications, especially in the presence of other mutations, such as *Flt3-ITD*. This view is consistent with *NPM1* being an histone chaperone that interacts with linker histone H1, plays a role in sperm chromatin remodeling, enhances acetylation-dependent chromatin transcription and controls ribosomal DNA gene transcription [13].

To assess the relevance of mouse findings to human AML, we correlated *GATA1* mRNA expression with the *NPM1* and *FLT3-ITD* mutational status in the BM of 47 AML, demonstrating that patients harboring both mutations displayed the lowest expression of *GATA1* (Fig. 2b i). The median *GATA1* level of 0.44 was arbitrarily used as cut-off to distinguish high and low expressing patients. AMLs with low *GATA1* were more frequent among *NPM1*-mutated/*FLT3-ITD* AMLs than unmutated, single *NPM1* or *FLT3-ITD*-mutated patients (72 vs 31, 46 and 57% respectively; pie charts in Fig. 2b i). These findings were further validated in an independent database of 266 AML of the Munich Leukemia Laboratory (www.ncbi.nlm.nih.gov/geo, accession number (GSE16015) (Figure S9). Additionally, we explored the methylation status of the *GATA1* promoter region in 24 patients, revealing a significant DNA methylation in *NPM1*-mutated/*FLT3-ITD* samples with an

average of $78.1\% \pm 1.3$ methylated CpG sites compared to $68.8\% \pm 2.6$ in *NPM1*-mutated only, $69\% \pm 0.7$ in *FLT3-ITD*-mutated only and $64\% \pm 3.1$ in wild-type (Fig. 2b ii). Finally, the analysis of GATA1 expression levels was performed in BM samples from 3 *NPM1*-mutated/*FLT3-ITD* patients treated with 5-Aza-dC, revealing a significant up-regulation of GATA1 mRNA after the first cycle (Fig. 2b iii). These data corroborate a potential role for DNA methylation of GATA1 promoter in the development of *NPM1*-mutated/*FLT3-ITD* AML. Our findings are also of potential clinical relevance, as GATA1 transcriptional response to 5-Aza-dC in mice results in significant improvement of the myeloid phenotype. Similarly, we observed GATA1 mRNA up-regulation in two *NPM1*-mutated/*FLT3-ITD* AML patients upon 5-Aza-dC treatment.

In conclusion, we identified deregulation of GATA1 as a new feature of *Npm1/Flt3-ITD* AML in mice and humans. This is an early event altering the HSC fate and sensitizing cells to further malignant transformation. Our model may also be valuable for further assessment of FLT3 inhibitors [14] and other drugs that have been shown to be active against *NPM1*-mutated AML [15].

Acknowledgements This work was supported by AIRC IG 2016 no.18568 (to BF), ERC Adv Grant 2016 no. 740230 (to BF) and ERC Cons Grant 2016 no. 725725 (to MPM).

Author contributions PS and BF conceived the study. LC, EV, RR, DS, CR, FS, BDP, CR and VG performed the experiments and analyzed the data. DS, DC, OB and LC performed cytometric analysis. LC, DS, RR and VG performed molecular analysis. EV, RR, FS and LC carried out histological analysis. PS and GS constructed analytical and visualization tools and databases. TH, provided samples. MPM and FF provided logistical support. PS and BF wrote the manuscript. All authors approved the manuscript.

Compliance with ethical standards

Conflict of interest BF applied for a patent on the clinical use of *NPM1* mutants. The other authors declare that they have no conflict of interest.

Publisher's note: Springer Nature remains neutral with regard to jurisdictional claims in published maps and institutional affiliations.

Open Access This article is licensed under a Creative Commons Attribution 4.0 International License, which permits use, sharing, adaptation, distribution and reproduction in any medium or format, as long as you give appropriate credit to the original author(s) and the source, provide a link to the Creative Commons license, and indicate if changes were made. The images or other third party material in this article are included in the article's Creative Commons license, unless indicated otherwise in a credit line to the material. If material is not included in the article's Creative Commons license and your intended use is not permitted by statutory regulation or exceeds the permitted

use, you will need to obtain permission directly from the copyright holder. To view a copy of this license, visit <http://creativecommons.org/licenses/by/4.0/>.

References

- Ley TJ, Miller C, Ding L, Raphael BJ, Mungall AJ, Robertson A, et al. Genomic and epigenomic landscapes of adult de novo acute myeloid leukemia. *N Engl J Med* 2013;368:2059–74.
- Falini B, Mecucci C, Tiacci E, Alcalay M, Rosati R, Pasqualucci L, et al. Cytoplasmic nucleophosmin in acute myelogenous leukemia with a normal karyotype. *N Engl J Med*. 2005;352:254–66.
- Sportoletti P, Grisendi S, Majid SM, Cheng K, Clohessy JG, Viale A, et al. *Npm1* is a haploinsufficient suppressor of myeloid and lymphoid malignancies in the mouse. *Blood*. 2008;111:3859–62.
- Khanna-Gupta A, Abayasekara N, Levine M, Sun H, Virgilio M, Nia N, et al. Up-regulation of translation eukaryotic initiation factor 4E in nucleophosmin 1 haploinsufficient cells results in changes in CCAAT enhancer-binding protein alpha activity: implications in myelodysplastic syndrome and acute myeloid leukemia. *J Biol Chem*. 2012;287:32728–37.
- Gale RE, Green C, Allen C, Mead AJ, Burnett AK, Hills RK, et al. The impact of FLT3 internal tandem duplication mutant level, number, size and interaction with *NPM1* mutations in a large cohort of young adult patients with acute myeloid leukemia. *Blood*. 2008;111:2776–84.
- Adolfsson J, Mansson R, Buza-Vidas N, Hultquist A, Liuba K, Jensen CT, et al. Identification of *Flt3+* lympho-myeloid stem cells lacking erythro-megakaryocytic potential a revised road map for adult blood lineage commitment. *Cell*. 2005;121:295–306.
- Ferreira R, Ohneda K, Yamamoto M, Philipsen S. GATA1 function, a paradigm for transcription factors in hematopoiesis. *Mol Cell Biol*. 2005;25:1215–27.
- Yoshida K, Toki T, Okuno Y, Kanezaki R, Shiraishi Y, Sato-Otsubo A, et al. The landscape of somatic mutations in Down syndrome-related myeloid disorders. *Nat Genet*. 2013;45:1293–9.
- Ayala R, Martinez-Lopez J, Gilsanz F. Acute myeloid leukemia and transcription factors: role of erythroid Kruppel-like factor (EKLF). *Cancer Cell Int*. 2012;12:25.
- Figuerola ME, Abdel-Wahab O, Lu C, Ward PS, Patel J, Shih A, et al. Leukemic *IDH1* and *IDH2* mutations result in a hypermethylation phenotype, disrupt *TET2* function, and impair hematopoietic differentiation. *Cancer Cell*. 2010;18:553–67.
- Kats LM, Reschke M, Taulli R, Pozdnyakova O, Burgess K, Bhargava P, et al. Proto-oncogenic role of mutant *IDH2* in leukemia initiation and maintenance. *Cell Stem Cell*. 2014;14:329–41.
- Shih AH, Jiang Y, Meydan C, Shank K, Pandey S, BarreYRO L, et al. Mutational cooperativity linked to combinatorial epigenetic gain of function in acute myeloid leukemia. *Cancer Cell*. 2015;27:502–15.
- Lindstrom MS. *NPM1/B23*: a multifunctional chaperone in ribosome biogenesis and chromatin remodeling. *Biochem Res Int*. 2011;2011:195209.
- Falini B, Sportoletti P, Brunetti L, Martelli MP. Perspectives for therapeutic targeting of gene mutations in acute myeloid leukaemia with normal cytogenetics. *Br J Haematol*. 2015;170:305–22.
- Falini B, Brunetti L, Martelli MP. Dactinomycin in *NPM1*-mutated acute myeloid leukemia. *N Engl J Med*. 2015;373:1180–2.